27

Humanoid Robots

27.1 Zero-Moment Point — Proper Interpretation
Introduction • The ZMP Notion • The Difference between ZMP and the Center of Pressure (CoP)

27.2 Modeling of Biped Dynamics and Gait Synthesis
Single-Support Phase • Double-Support Phase • Biped Dynamics • Example

27.3 Control Synthesis for Biped Gait
Synthesis of Control with Limited Accelerations • Synthesis of Global Control with Respect to ZMP Position • Example

27.4 Dynamic Stability Analysis of Biped Gait
Modeling of Composite Subsystems • Stability Analysis • Example

27.5 Realization of Anthropomorphic Mechanisms and Humanoid Robots
Active Exoskeletons • Humanoid Robots • Virtual Humanoid Robot Platform • New Application of the ZMP Concept in Human Gait Restoration

27.6 Conclusion

Miomir Vukobratović
Mihajlo Pupin Institute

Branislav Borovac
University of Novi Sad

Dragoljub Šurdilović
Fraunhofer Institute

Dragan Stokić
ATB Institute

During the last several years, significant stagnation has been observed in the development and application of industrial robots. The reason for this lies in the fact that in the last two or three decades a majority of simpler jobs in different industries and in workplaces presenting hostile environments to humans have been robotized.

We are now in an era of specialized, unconventional robots dedicated to complex tasks to be performed under specific and hazardous conditions. These robots are endowed with the elements of artificial intelligence. The objective is to initiate long-term multidisciplinary research with the goal of designing function-oriented devices equipped with proper onboard intelligence capable of autonomously performing common human work.

It is expected that the new generation of robots will yield explosive development that will have an impact comparable to that we witnessed with the appearance of personal computers. The present service robots will be replaced by personal robots. From the scientific point of view they will represent the continuation of the earlier research on anthropomorphic robots (now called humanoid robots) that are endowed with elements of artificial intelligence. The future service robots will work in the environment of humans, which imposes the requirement for human-like behavior in the area of motion, intelligence, and communication. Obviously, modeling, control, and design of such robots must be based on a wide range of disciplines such as system theory, artificial intelligence, material science, mechanics, and even biomechanics, physiology, and neuroscience.

27.1 Zero-Moment Point — Proper Interpretation

27.1.1 Introduction

Biped locomotion has been at the focus of researchers for decades. Theoretical studies have been followed by simulations and realizations — from the simplest cases of planar mechanisms to humanoid robots, which are the most complex locomotion mechanisms constructed to date. Irrespective of their structures and complexities, the basic characteristics of all locomotion systems are: (1) the presence of unpowered degrees of freedom (DOFs) formed by the contact of the foot with the ground surface, (2) gait repeatability (symmetry), and (3) regular interchangeability of the number of legs that are simultaneously in contact with the ground. Two different situations arise in sequence during walking: the statically stable double-support phase in which the mechanism is supported on both feet simultaneously, and the statically unstable single-support phase when only one foot of the mechanism is in contact with the ground and the other is transferred from the back to front position. Thus, the locomotion mechanism changes its structure from an open to a closed kinematic chain during a single walking cycle. All these circumstances have to be taken into account in gait synthesis.

All of the biped mechanism joints are powered and directly controllable except for the joint formed by contact of the foot and the ground. This contact is essential for walking because this is the only point at which the mechanism interacts with the environment, and the mechanism's position relative to the environment depends on the regularity of its behavior. It is often called unpowered DOF because in case of an improper motion, the mechanism as a whole would start to rotate about the foot edge, and a new unpowered joint would appear. If such improper foot behavior occurred, the position of the entire mechanism relative to the environment would be jeopardized and the mechanism would overturn.

Foot behavior cannot be controlled directly; it is controlled in an indirect way by ensuring appropriate dynamics of the mechanism above the foot. Thus, the overall indicator of mechanism behavior is the ground reaction force: its intensity, direction, and particularly its acting point, termed the *zero-moment point* (ZMP).[1-5] Recognition of the significance and role of ZMP in the biped artificial walk was a turning point in gait planning and control. The methods for gait synthesis (semi-inverse method) were proposed in the two seminal works,[1-2] and for a long time they remained the only mechanisms for biped gait synthesis. Recently, another method has been reported,[6] which, among other criteria, takes into account the overall gait indicator: the ZMP position.

The concept of ZMP has recently found practical applications in humanoid, biped, and multi-legged robots. Numerous studies addressed the mathematical formalisms for computing the ZMP. Several algorithms for biped control and monitoring based on the ZMP concept have been proposed (e.g., Inoue et al.,[7] Huang et al.,[8] Yagi and Lumelsky.[9] Fujimoto et al.,[10] and Fukuda et al.[11]). As demonstrated recently,[12] the ZMP is also convenient for the analysis and control of human gait in rehabilitation robotics. The ZMP concept provides a useful dynamic criterion for the analysis and synthesis of human/humanoid robot locomotion. The ZMP indicates gait balance during the entire gait cycle and provides a quantitative measure for the unbalanced moment about the support foot and for the robustness (balancing margin) of the dynamic gait equilibrium.

27.1.2 The ZMP Notion

First, we would like to clarify the notion and, accordingly, the name of ZMP. Let us consider the single-support phase as shown in Figure 27.1, i.e., when only one foot is in contact with the ground (stance leg) while the other is in the swing phase, passing from the back to the front position. To maintain the mechanism's dynamic equilibrium, the ground reaction force $\bar{\mathbf{R}}$ should act at the appropriate point on the foot sole to balance all the forces acting on the mechanism during motion (inertial, gravitational, Coriolis, and centrifugal forces, and the corresponding moments), as shown in Figure 27.1.

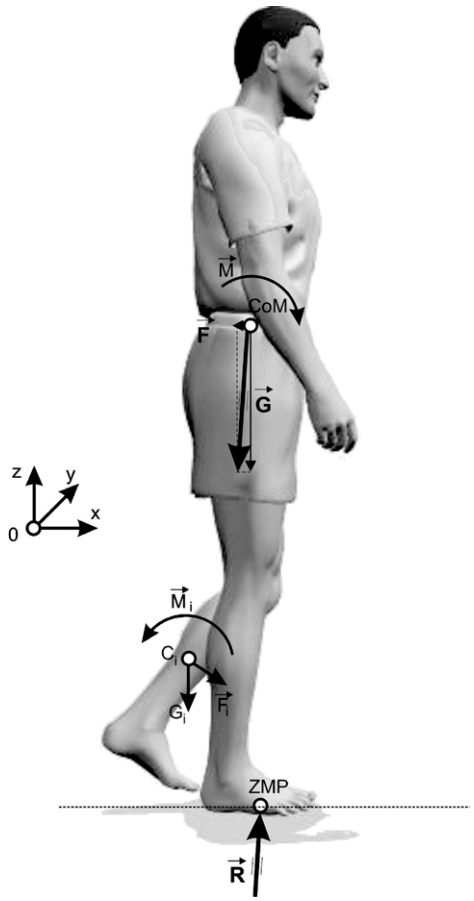

FIGURE 27.1 Single-support phase.

If we place the coordinate system at the point where $\vec{\mathbf{R}}$ is acting (let us assume that this point is under the foot), it is clear from the equilibrium conditions that the moments acting about the horizontal axes x and y will always be equal to zero, i.e., $M_x = 0$ and $M_y = 0$. The only moment component that may exist is M_z. It is realistic to assume that the friction coefficient between the ground and the foot is high enough and that M_z is balanced by friction forces. Thus, M_z will not cause foot motion and change in foot dynamics, and will not influence behavior of the mechanism above the foot. Since both moments relevant to the gait continuation (M_x and M_y) equal zero, a natural name for the ground reaction force acting at this point will be the zero moment point. Any change in the locomotion dynamics will change the vector of the ground reaction force, causing simultaneous changes in its direction, intensity, and acting point (ZMP). The following basic ZMP definition[1,2,13] reflects the above consideration:

Definition 1 (ZMP): The pressure under the supporting foot can be replaced by the appropriate reaction force acting at a certain point of the mechanism's foot. Since the sum of all moments of active forces with respect to this point is equal to zero, it is termed the zero-moment point (ZMP).

To define ZMP in a mathematical form, let us consider the dynamic model of the human, humanoid, or biped robot (the following analysis can be applied to all these systems). The human/humanoid dynamics will be modeled using the multibody system model consisting of N chains involving the body parts (head, arms, legs, trunk, and pelvis). Each chain consists of n_i-links (i = 1,…,N) interconnected with single DOF joints (the multiple DOF joints are decomposed into

the single ones). For the sake of simplicity, let us consider the rigid body model that is a relatively good approximation of the humanoid dynamics, though it represents a very idealized model of the human gait. The multi-DOF structures of the human locomotion mechanism, joint flexibility, and structural and behavioral complexity of the foot support the realization of dynamic gait patterns that are difficult to achieve with the existing humanoid systems.

During locomotion the following active motion forces act on the body links:

$\vec{\mathbf{G}}_i$ = Gravitation force of the i-th link acting at the mass center C_i
$\vec{\mathbf{F}}_i$ = Inertial force of the i-th link acting at the mass center C_i
$\vec{\mathbf{M}}_i$ = Moment of the inertial force of the i-th link for C_i
$\vec{\mathbf{R}}$ = Resultant ground reaction force

All active motion forces (gravitational and inertial forces and moments) can be replaced by main resultant gravitation and inertial force and, in most cases, resultant inertial moment reduced at body center of mass (CoM). The ground reaction force and moment can be decomposed into vertical and horizontal components with respect to the reference frame. The horizontal reaction force represents the friction force essential for preserving the contact between the foot and the ground. The vertical reaction moment represents the moment of the friction reaction forces reduced at an arbitrary point P. We will assume a stable foot–floor contact without sliding. This means that the static friction forces compensate for the corresponding dynamic body reaction forces. Accordingly, the vertical reaction force and horizontal reaction moment components represent the dynamic reaction forces that are not compensated by the friction. The decomposition will be presented in the following form:

$$\begin{aligned}\vec{\mathbf{R}} &= \vec{\mathbf{R}}_v + \vec{\mathbf{R}}_f \\ \vec{\mathbf{M}} &= \vec{\mathbf{M}}_h + \vec{\mathbf{M}}_f\end{aligned} \tag{27.1}$$

where the indices h and v denote the horizontal and vertical components respectively, while f indicates the friction reaction force and moment components. Let us select the ZMP as the reduction point of interest, i.e., $P = ZMP$. Then the following equations express the dynamic equilibrium during the motion in the reference coordinate system:

$$\begin{aligned}&\vec{\mathbf{R}}_v + \vec{\mathbf{R}}_f + \sum_{j=1}^{N}\sum_{i=1}^{n_j}\left(\vec{\mathbf{F}}_i + \vec{\mathbf{G}}_i\right) = 0 \\ &\overrightarrow{OZMP} \times \vec{\mathbf{R}} + \sum_{j=1}^{N}\sum_{i=1}^{n_j}\overrightarrow{OC_i} \times \left(\vec{\mathbf{F}}_i + \vec{\mathbf{G}}_i\right) + \sum_{j=1}^{N}\sum_{i=1}^{n_j}\vec{\mathbf{M}}_i + \vec{\mathbf{M}}_{hZMP} + \vec{\mathbf{M}}_{fZMP} = 0\end{aligned} \tag{27.2}$$

where O denotes the origin of the reference frame (Figure 27.1). Then, based on the ZMP definition we have:

$$\vec{\mathbf{M}}_{hZMP} = 0\,. \tag{27.3}$$

Substituting the relation:

$$\overrightarrow{OC_i} = \overrightarrow{OZMP} + \overrightarrow{ZMPC_i} \tag{27.4}$$

into the second equation of Equation (27.2) and taking into account the first equation of (27.2) gives:

$$\sum_{j=1}^{N}\sum_{i=1}^{n_j}\overrightarrow{ZMPC_i}\times\left(\vec{\mathbf{F}}_i+\vec{\mathbf{G}}_i\right)+\sum_{j=1}^{N}\sum_{i=1}^{n_j}\vec{\mathbf{M}}_i+\vec{\mathbf{M}}_{fZMP}=0\,. \tag{27.5}$$

Considering only the dynamic moment equilibrium in the horizontal ground plane (i.e., the moments that are not compensated by friction), we can write:

$$\left(\sum_{j=1}^{N}\sum_{i=1}^{n_j}\overrightarrow{ZMPC_i}\times\left(\vec{\mathbf{F}}_i+\vec{\mathbf{G}}_i\right)+\sum_{j=1}^{N}\sum_{i=1}^{n_j}\vec{\mathbf{M}}_i\right)_h=0\,. \tag{27.6}$$

Substituting Equation (27.4) in Equation (27.6) yields:

$$\left(\overrightarrow{OZMP}\times\sum_{j=1}^{N}\sum_{i=1}^{n_j}\left(\vec{\mathbf{F}}_i+\vec{\mathbf{G}}_i\right)\right)_h=\left(\vec{\mathbf{R}}\times\overrightarrow{OZMP}\right)_h=\left(\sum_{j=1}^{N}\sum_{i=1}^{n_j}\overrightarrow{OC_i}\times\left(\vec{\mathbf{F}}_i+\vec{\mathbf{G}}_i\right)+\sum_{j=1}^{N}\sum_{i=1}^{n_j}\vec{\mathbf{M}}_i\right)_h \tag{27.7}$$

Equations (27.6) and (27.7) represent the mathematical interpretation of ZMP and provide the formalism for computing the ZMP coordinates in the horizontal ground plane.

The one-step cycle consists of the single- and double-support phases, taking place in sequence. A basic difference between these elemental motion phases is that during the motion in the single-support phase, the position of the free foot is not fixed relative to the ground. In the double-support phase, the positions of both feet are fixed. From the ZMP point of view, the situation is identical. In both cases, ZMP should remain within the support polygon in order to maintain balance. During the gait (let us call it *balanced gait* to distinguish it from the situation when equilibrium of the system is jeopardized and the mechanism collapses by rotating about the support polygon edge), the ground reaction force acting point can move only within the support polygon. The gait is balanced when and only when the ZMP trajectory remains within the support area. In this case, the system dynamics is perfectly balanced by the ground reaction force and overturning will not occur. In the single-support phase, the support polygon is identical to the foot surface. In the double-support phase, however, the size of the support polygon is defined by the size of the foot surface and by the distance between them (the convex hulls of the two supporting feet).

This ZMP concept is primarily related to the gait dynamics; however it can also be applied to consider static equilibrium when the robot maintains a certain posture. The only difference is in the forces inducing the ground reaction force vector. In the static case, there is only the mechanism weight, while the gait also involves dynamic forces. Accordingly, when equilibrium of a static posture (the mechanism is frozen in a certain posture and no gait is performed) is considered, the vertical projection of total active force acting at the mass center must be within the support polygon. This is a well-known condition for static equilibrium.

27.1.3 The Difference between ZMP and the Center of Pressure (CoP)

One can see from the above analysis that ZMP is apparently equivalent to the center of pressure (CoP), representing the application point of the ground reaction forces (GRFs). The CoP can be defined as:

Definition 2 (CoP): CoP represents the point on the support foot polygon at which the resultant of distributed foot ground reaction forces acts.

The CoP is commonly used in human gait analysis based on force platform or pressure mat measurements. In human locomotion, the CoP changes during the stance phase, generally moving from the heel toward a point between the first and second metatarsal heads. It is relatively simple to demonstrate that in the considered single-support phase and for balanced dynamic gait equilibrium

(Figure 27.1), the ZMP coincides with the CoP. Let us again consider the equilibrium (Equation (27.2)) assuming that CoP is the reduction point P = CoP and ZMP and CoP do not coincide. According to the adopted notation, the force and moment reduced at CoP are denoted as $-\vec{\mathbf{R}}$ and $-\vec{\mathbf{M}}_{CoP}$ respectively, while the reaction force and moment are $\vec{\mathbf{R}}$ and $\vec{\mathbf{M}}_{CoP}$. Consider the equilibrium of the foot reaction forces, supposing that ZMP does not coincide with CoP. For this case we can write:

$$\left(\overrightarrow{ZMPCoP} \times \vec{\mathbf{R}} + \vec{\mathbf{M}}_{CoP}\right)_h = 0 \tag{27.8}$$

However, on the basis of CoP definition for the balanced gait, we have:

$$\left(\vec{\mathbf{M}}_{CoP}\right)_h = 0 \tag{27.9}$$

which can only be satisfied if:

$$\overrightarrow{ZMPCoP} = 0 \tag{27.10}$$

and it follows that $ZMP \equiv CoP$.

Let us discuss the justification of introducing a new term (ZMP) for a notion that has already been known in technical practice (CoP). While CoP is a general term encountered in many technical branches (e.g., fluid dynamics), ZMP expresses the essence of this point that is used exclusively for gait synthesis and control in the field of biped locomotion. It reflects much more clearly the nature of locomotion. For example, in the biped design we can compute ZMP on the assumption that the support polygon is large enough to encompass the calculated acting point of the ground reaction force. Then we can determine the form and dimension of the foot-supporting area encompassing all ZMP points or, if needed, we can change the biped dynamic parameters or synthesize the nominal gait and control the biped to constantly keep ZMP within the support polygon.

Furthermore, the ZMP has a more specific meaning than CoP in evaluating the dynamics of gait equilibrium. To show the difference between ZMP and CoP, let us consider the dynamically unbalanced single-support situation (the mechanism as a whole rotates about the foot edge and overturns) illustrated in Figure 27.2, which is characterized by a moment about CoP that could not be balanced by the sole reaction forces. The reaction moment that can be generated between the foot and the ground is limited due to the unilateral contact between each sole and the floor. The intensity of balancing moments depends on the foot dimension. Obviously, it is easier for a person with larger sole to balance the gait. The dynamic motion moments in specific cases may exceed the limit, causing the foot to leave the ground. In spite of the existence of a nonzero supporting area (soft human/humanoid foot), reaction forces cannot balance the system in such a case. The way in which this situation in human/humanoid gait can occur will be considered later. As is clear from Figure 27.2, the CoP and the ZMP do not coincide in this case. Using an analogy to fluid dynamics, we could determine CoP as the center of pressure distribution (e.g., obtained by a pressure mate). It should be mentioned that in regular human gait, in a dynamic transition phase (e.g., heel strike and toe off), it is difficult to estimate CoP on the basis of force plate measurements.

However, ZMP, even in the case illustrated in Figure 27.2, can be uniquely determined on the basis of its definition. Assuming that both reaction force and unbalanced moment are known, we can mathematically replace the force–moment pair with a pure force displaced from the CoP. In this situation, however, the ZMP and the assigned reaction force have a pure mathematical/mechanical meaning (obviously, the ZMP does not coincide with the CoP) and the ZMP does not represent a physical point. However, the ZMP location outside the support area (determined by the vector $\vec{\mathbf{r}}$ in Figure 27.2) provides very useful information for gait balancing. The fact that ZMP is instantaneously on the edge or has left the support polygon indicates the occurrence of an unbalanced

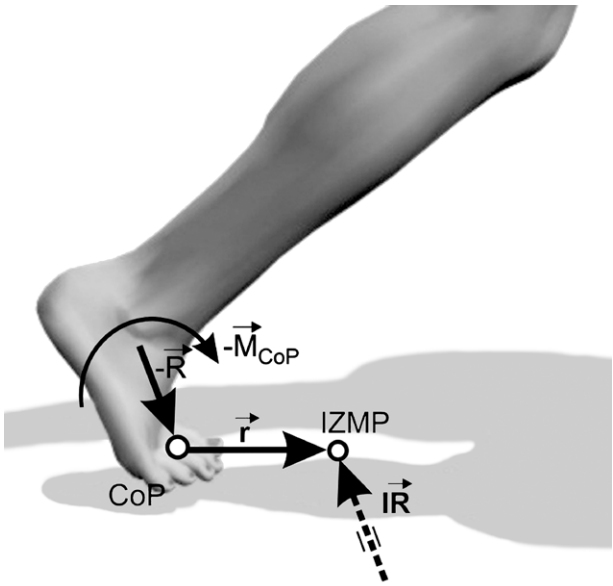

FIGURE 27.2 Action/reaction forces at CoP and ZMP (irregular case).

moment that cannot be compensated for by foot reaction forces. The distance of ZMP from the foot edge provides the measure for the unbalanced moment that tends to rotate the human/humanoid around the supporting foot and, possibly, to cause a fall. When the system encounters such a hazardous situation, it is still possible by means of a proper dynamic corrective action of the biped control system to bring ZMP into the area where equilibrium is preserved. To avoid this, a fast rebalancing by muscles or actuator actions (change of dynamic forces acting on the body) is needed. Several approaches to realization of this action have been discussed.[13]

On the basis of the above discussion, it is obvious that generally the ZMP does not coincide with the CoP

$$ZMP \neq CoP. \tag{27.11}$$

The CoP may never leave the support polygon. However, the ZMP, even in the single-support gait phase, can leave the polygon of the supporting foot when the gait is not dynamically balanced by foot reaction forces, e.g., in the case of a nonregular gait (even in the case of a degenerative gait). Hence, ZMP provides a more convenient dynamic criterion for gait analysis and synthesis.

The ZMP outside the support polygon indicates an unbalanced (irregular) gait and does not represent a physical point related to the sole mechanism. It can be referred to as imaginary ZMP (IZMP). Three characteristic cases for the nonrigid foot in contact with the ground floor, sketched in Figure 27.3, can be distinguished. In the so-called regular (balanced and repetitive) gait, the ZMP coincides with CoP (Figure 27.3a). If a disturbance brings the acting point of the ground reaction force to the foot edge, the perturbation moment will cause rotation of the complete biped locomotion system about the edge point (or a very narrow surface, under the assumption that the sole of the shoe is not fully rigid) and overturning (Figure 27.4). In that case we speak of IZMP, whose imaginary position depends on the intensity of the perturbation moment (Figure 27.3b). However, it is possible to realize the biped motion, for example, on the toe tips (Figure 27.3c) with special shoes having pinpoint areas (balletic locomotion), while keeping the ZMP position within the pinpoint area. Although it is not a regular (conventional, ordinary) gait, the ZMP also coincides with CoP in that case.

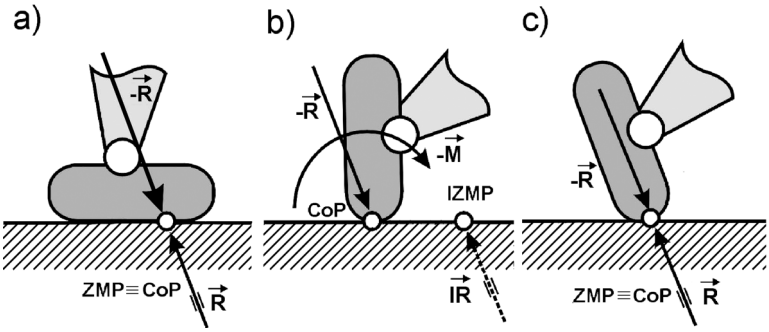

FIGURE 27.3 The possible relative positions of ZMP and CoP: (a) dynamically balanced gait, (b) unbalanced gait (the system rotates about the foot-edge and overturns), and (c) intentional foot-edge equilibrium (balletic locomotion).

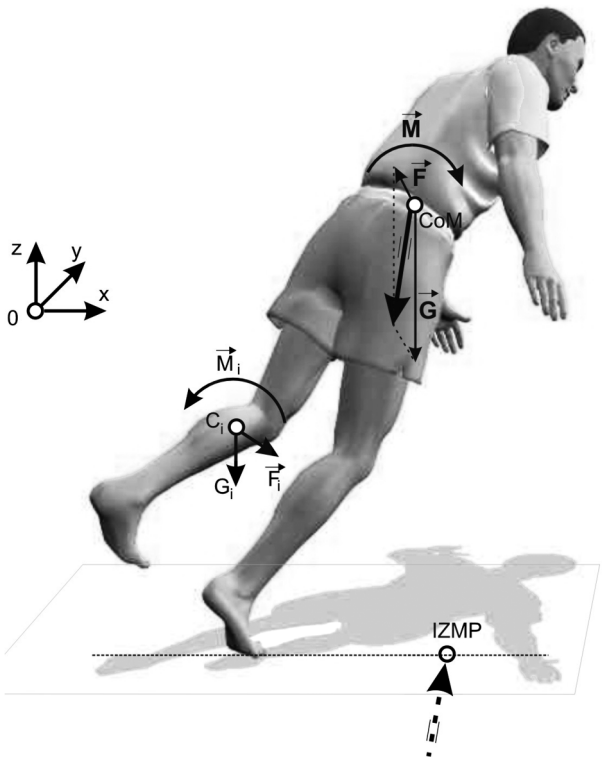

FIGURE 27.4 Imaginary ZMP in unbalanced human gait.

Because of foot elasticity and the complex form of the supporting area, the ZMP displacements outside the safe zone (Figure 27.2) in human locomotion are much more complex and difficult to model. Even in a regular human gait, ZMP leaves the support polygon dynamically during the transition from the single- to double-support phase, providing a smooth dynamic locomotion. The implementation of such gait patterns in humanoids with simple rigid feet is not practically possible.

In the double-support phase, and even more during transition from the single to the double phase, the ZMP leaves the foot-supporting polygon. Stable dynamic equilibrium in the double-support phase is characterized by the ZMP location within the enveloping polygon between the two feet.[13]

The extent of ZMP dislocation from the enveloping polygon also provides a practical measure for the unbalanced moments. In previous works[13] our attention has mainly been focused on the problems of biped design and nominal motion synthesis, as well as stability analysis and biped dynamic control that will prevent the ZMP excursions close to the edges of the supporting polygon in spite of various disturbances and model uncertainties. Due to limitations of the sensory and control systems, the occurrence of a new unpowered joint (ZMP at the edges of the support polygon) has been considered as critical and undesirable in the past.

Hence, the situation when ZMP can arbitrarily be located in the foot plane was practical in designing the biped foot dimensions and nominal motion synthesis. When the ZMP approaches critical areas or even abandons the support polygon (Figure 27.3), balancing is focused primarily on compensating for the unbalanced dynamic moment using the posture control. One way of overcoming such critical situation is to switch to a new nominal trajectory that is closest to the momentary system state.[5] These nominals are synthesized to bring the system back to the stationary state and enable gait continuation. To do this, it is not necessary to have information about exact intensity of the disturbance moment. For such an approach (which is very close to the human behavior in similar situations), it suffices to detect the occurrence of such hazardous situations. Thus, there is no need for on-line computation of the IZMP location for the purpose of biped control. For these reasons the IZMP location has not gained more practical importance. However, the recent development of powerful control and sensory systems and the fast expansion of humanoid robots gives a new significance to the IZMP, particularly in rehabilitation robotics. The consideration of ZMP locations, including also the areas outside the supporting foot sole, becomes essential for rehabilitation devices.[12]

27.2 Modeling of Biped Dynamics and Gait Synthesis

The synthesis of the motion of humanoid robots requires realization of a human-like gait. There are several possible approaches, depending on the type of locomotion activity involved. It should be kept in mind that the skeletal activity of human beings is extremely complex and involves many automated motions. Hence, the synthesis of the artificial locomotion–manipulation motion has complexities related to the required degree of mimicking of the corresponding human skeletal activity.

If, however, we concentrate on the synthesis of a regular (repeatable) gait, then it is natural to copy the trajectories of the natural gait and impose them onto the artificial (humanoid) system. Of course, the transfer of trajectories (in this case of the lower limbs) from a natural to an artificial system can be realized with a higher or lower degree of similarity to the human gait. Hence, the anthropomorphism of artificial gait represents a serious problem. To explain the practical approach to solving this problem, let us assume we have adopted one of the possible gait patterns. By combining the adopted (prescribed) trajectories of the lower limb joints (method of prescribed synergy[1,2,5,13]) and the position (trajectory) of ZMP using the semi-inverse method,[2,5,13] it is possible to determine the compensation motion of the humanoid robot from the moments about the corresponding axes for the desired position of the ZMP (or ZMP trajectory). The equilibrium conditions can be written also for the arm joints. In fact, the unpowered arm joints represent additional points where moments are known (zero). These supplementary moment equations about the unpowered arm axes yield the possibility of including passive arms in the synthesis of dynamically balanced humanoid gait.

27.2.1 Single-Support Phase

Let us suppose the system is in single-support phase and the contact with the ground is realized by the full foot (Figure 27.5). It is possible to replace all vertical elementary reaction forces by the resultant force R_V. Only regular gait will be considered, and the ZMP position has to remain within the support area (polygon).

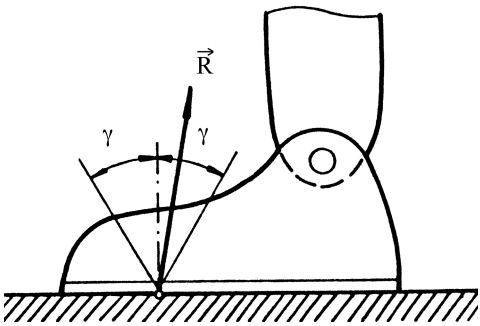

FIGURE 27.5 Longitudinal distribution of pressure on the foot and ZMP position.

The basic idea of artificial synergy synthesis is that the law of the change of total reaction force under foot is known in advance or prescribed. The prescribed segments of the dynamic characteristics which restrict the system in a dynamic sense are called dynamic connections. If a certain point represents the ZMP and the ground reaction forces $\vec{R}_V$ is reduced to it, then the moment $\vec{M}$ should be equal to zero. The vector $\vec{M}$ always has a horizontal direction and, hence, two dynamic conditions have to be satisfied: the projection of the moment on the two mutually orthogonal axes X and Y in the horizontal plane should be equal to zero.

$$M_X = 0 \quad M_Y = 0 \tag{27.12}$$

As far as friction forces are concerned, it is a realistic assumption that the friction coefficient is sufficiently large to prevent slippage of the foot over the ground surface. Thus, it can be stated that their moment with respect to the vertical axis V is equal to zero:

$$M_V = 0\,. \tag{27.13}$$

The axis V can be chosen to be in any place, but if it passes through the ZMP, then the axes X, Y, and V constitute an orthogonal coordinate frame, and V will be denoted by Z. The external forces acting on the locomotion system are the gravity, friction, and ground reaction forces. Let us reduce the inertial forces and moments of inertial forces of all the links to the ZMP and denote them by $\vec{F}$ and $\vec{M}_F$, respectively. The system equilibrium conditions can be derived using D'Alembert's principle and conditions (27.12) can be rewritten as:

$$(\vec{M}_G + \vec{M}_F)\cdot\vec{e}_X = 0\,, \quad (\vec{M}_G + \vec{M}_F)\cdot\vec{e}_Y = 0 \tag{27.14}$$

where $\vec{M}_G$ is the total moment of gravity forces with respect to ZMP, while $\vec{e}_X$ and $\vec{e}_Y$ are unit vectors of the x and y axes of the absolute coordinate frame. The third equation of dynamic connections, Equation (27.13), becomes:

$$(\vec{M}_F + \vec{\rho} \times \vec{F}\,)\cdot\vec{e}_V = 0 \tag{27.15}$$

where $\vec{\rho}$ is a vector from ZMP to the piercing point of the axis V through the ground surface; $\vec{e}_v$ is a unit vector of the axis V.

Let us adopt the relative angles between two links to be the generalized coordinates and denote them by q^i. Suppose the mechanism foot rests completely on the ground, so that the angle is zero, $q_0 \equiv 0$. The inertial force $\vec{F}$ and the moment $\vec{M}_F$, in general, can be represented in the linear forms of the generalized accelerations and quadratic forms of generalized velocities:

$$F^k = \sum_{i=1}^{n} a_i^k \cdot \ddot{q}^i + \sum_{i=1}^{n} \sum_{j=1}^{n} b_{ij}^k \cdot \dot{q}^i \dot{q}^j, \; k = 1, 2, 3$$

$$M_F^k = \sum_{i=1}^{n} c_i^k \cdot \ddot{q}^i + \sum_{i=1}^{n} \sum_{j=1}^{n} d_{ij}^k \cdot \dot{q}^i \dot{q}^j, \; k = 1, 2, 3 \tag{27.16}$$

where the coefficients $a_i^k, b_{ij}^k, c_i^k, d_{ij}^k$ (k = 1, 2, 3; and = 1, …, n; j = 1, … n) are the functions of the generalized coordinates, and F^k and M_F^k (k = 1, 2, 3) denote projections of the vectors $\vec{F}$ and $\vec{M}_F$ onto the coordinate axes. By introducing these expressions into Equations (27.14) and (27.15) one obtains:

$$\vec{M}_G \cdot \vec{e}_x + \sum_{i=1}^{n} c_i^1 \cdot \ddot{q}^i + \sum_{i=1}^{n} \sum_{j=1}^{n} d_{ij}^1 \cdot \dot{q}^i \dot{q}^j = 0$$

$$\vec{M}_G \cdot \vec{e}_y + \sum_{i=1}^{n} c_i^2 \cdot \ddot{q}^i + \sum_{i=1}^{n} \sum_{j=1}^{n} d_{ij}^2 \cdot \dot{q}^i \dot{q}^j = 0 \tag{27.17}$$

$$\sum_{i=1}^{n} c_i^3 \cdot \ddot{q}^i + \sum_{i=1}^{n} \sum_{i=j}^{n} d_{ij}^3 \cdot \dot{q}^i \dot{q}^j + \rho^x \left(\sum_{i=1}^{n} a_i^2 \cdot \ddot{q}^i + \sum_{i=1}^{n} \sum_{i=1}^{n} b_{ij}^2 \cdot \dot{q}^i \dot{q}^i \right) - \rho^y \left(\sum_{i=1}^{n} a_i^1 \cdot \ddot{q}^i + \sum_{i=1}^{n} \sum_{j=1}^{n} b_{ij}^1 \cdot \dot{q}^i \dot{q}^j \right) = 0$$

where the superscripts x and y denote the components in direction of the corresponding axis.

If the biped locomotion system has only three DOFs, the trajectories for all angles q^i can be computed from Equation (27.17). If the system has more than three DOFs (and this is actually the case), the trajectories for the rest (n-3) coordinates should be prescribed in such a way to ensure the desired legs trajectories (for example, measured from the human walk). The trajectories for this part of the system are prescribed, while the dynamics of the rest of the system (i.e., the trunk and arms) are determined in a such a way to ensure the dynamic balance of the overall mechanism.

The set of coordinates can be divided in two subsets: one containing all the coordinates whose motion is prescribed, denoted as q^{0i}, and the other comprising all the coordinates whose motion is to be defined using the semi-inverse method,[1,13] denoted as q^{xi}. Accordingly, the condition (27.17) becomes:

$$\sum_{i=1}^{n} c_i^k \cdot \ddot{q}^{xi} + \sum_{i=1}^{n} \sum_{j=1}^{n} d_{ij}^k \cdot \dot{q}^{xi} \dot{q}^{xj} + g^k = 0, \; k = 1, 2, 3 \tag{27.18}$$

where c_i^k and d_{ij}^k (k = 1, 2, 3) are the vector coefficients dependent on q^0 and q^x, whereas the vector g^k (k = 1, 2, 3) is a function of q^0, $\dot{q}^0$, $\ddot{q}^0$, and q^x. Since the gait is symmetric, the repeatability conditions can be written in the form:[1,13]

$$q^i(0) = \pm q^i\left(\frac{T}{2}\right), \quad \dot{q}^i(0) = \pm \dot{q}^i\left(\frac{T}{2}\right)$$

where the sign depends on the physical nature of the appropriate coordinates and their derivatives; $(T/2)$ is the duration of one half-step. As the motion of the prescribed part of the mechanism has been already defined (repeatability conditions are implicitly satisfied), the repeatability conditions:

$$q^{xi}(0) = \pm q^{xi}\left(\frac{T}{2}\right), \quad \dot{q}^{xi}(0) = \pm \dot{q}^{xi}\left(\frac{T}{2}\right) \tag{27.19}$$

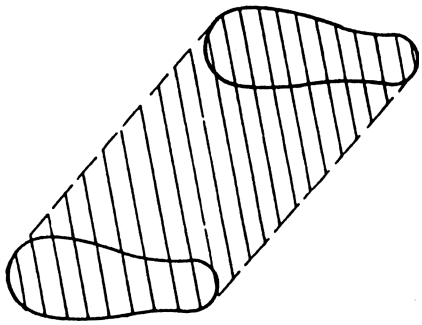

FIGURE 27.6 Double-support phase.

for the rest of the mechanism are to be added to the original set of equations describing the mechanism motion.

The system of Equation (27.18), together with the conditions (27.19), enables one to obtain the necessary trajectories of the coordinates q^{xi}, i.e., to carry out compensation synergy synthesis. After the synergy synthesis is completed, the driving torques that force the system to follow the nominal trajectories have to be computed.

27.2.2 Double-Support Phase

In the double-support phase, both mechanism feet are simultaneously in contact with the ground. The kinematic chain playing the role of the legs is closed, i.e., the unknown reaction forces to be determined act on both ends.

The procedure for the synergy synthesis is in the most part analogous to that for the single-support phase. Let the position of the axis V be selected within the dashed area in Figure 27.6. Then, by writing the equilibrium equations with respect to the three orthogonal axes passing through ZMP and setting the sum of all the moments of external forces to zero, the compensating movements for the corresponding part of the body can be computed.

The next problem is how to choose the position of the axis V with respect to the ZMP. The information on ZMP and axis V is insufficient for computation of the driving torques. For this reason, it is necessary to provide some additional relations concerning the ground reaction force. The total reaction force under one foot can be expressed as a sum of three reaction forces and moment components in the direction of coordinate axes. The components M_X and M_Y can be equal to zero since the vertical forces on the diagram are of the same sign. The third component M_V should also be equal to zero, according to the following consideration. Generally speaking, friction forces can produce moments, but in synergy synthesis, the moment M_V should also be equal to zero. Consequently, if the moments of friction forces are generated, they should be of the opposite sign under each foot. However, these moments do not affect the system motion but only load the leg drives and joints additionally. Because of that, it is reasonable to synthesize the gait in such a way to reduce each of these moments to zero. Thus it can be assumed that total moments of reaction forces under each foot are equal to zero:

$$\vec{M}_a = \vec{M}_b = 0 \tag{27.20}$$

where the subscripts a and b denote the left and right foot, respectively.

Characteristics of the friction between the foot and the ground can be represented by a friction cone (Figure 27.7). If the total ground reaction force $\vec{R}$ is within the cone of the angle 2γ, its horizontal component (i.e., friction force) will be of sufficient intensity to prevent an unwanted horizontal motion of the supporting foot over the ground surface. This can be expressed as:[13]

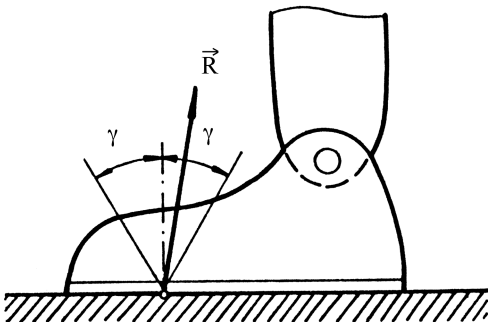

FIGURE 27.7 Friction cone.

$$\frac{\left|\vec{R}_x + \vec{R}_y\right|}{\left|\vec{R}_v\right|} \le tg\gamma = \mu \tag{27.21}$$

where μ is the friction coefficient of the surfaces in contact. Thus, it is reasonable to distribute the horizontal components of ground reaction forces per foot proportionally to the normal pressure. The vertical components are inversely proportional to the distances between the ZMP and the corresponding foot, so:

$$\frac{\left|\vec{R}_{v_a}\right|}{\left|\vec{R}_{v_b}\right|} = \frac{\ell_b}{\ell_a} \tag{27.22}$$

Then, from Equation (27.21) the relation:[4,13]

$$\frac{\left|\vec{T}_a\right|}{\left|\vec{T}_b\right|} = \frac{\ell_b}{\ell_a} \tag{27.23}$$

holds for the horizontal components, where $\vec{T}_a$ and $\vec{T}_b$ are the friction forces under the corresponding foot (Figure 27.8). On the basis of similarity of the triangles Δ OAD and Δ OBC, it can be concluded that the relation (27.23) does not depend on the direction of the force $\vec{T}$ (i.e., the distances ℓ'_a and ℓ'_b), but only on the distances between the feet, ℓ_a and ℓ_b. Thus, in order to have friction forces divided in proportion to the vertical pressures, a necessary and sufficient condition is that the axes ℓ'_a and ℓ'_b pass through the ZMP. Then, for synergy synthesis in the double-support phase, the following vector equation holds:

$$\sum_{i=1}^{n}\left(\vec{r}_i \times \left(\vec{G}_i + \vec{F}_i\right) + \vec{M}_i\right) = 0 \tag{27.24}$$

where $\vec{r}_i$ is a radius vector from the ZMP to the gravity center of the *i*-th link and $\vec{F}_i$ and $\vec{M}_i$ are the inertial force and corresponding moment of the *i*-th link reduced to its center of gravity.

When the synthesis of the compensating laws of motion is completed, it is possible to determine the total horizontal and vertical reactions:

$$R_Z = -\sum_{i=1}^{n}\left(\vec{F}_{iZ} + \vec{G}_i\right), \quad \vec{T} = \sum_{i=1}^{n}\left(\vec{F}_{iX}\cdot\vec{e}_X + \vec{F}_{iY}\cdot\vec{e}_Y\right) \tag{27.25}$$

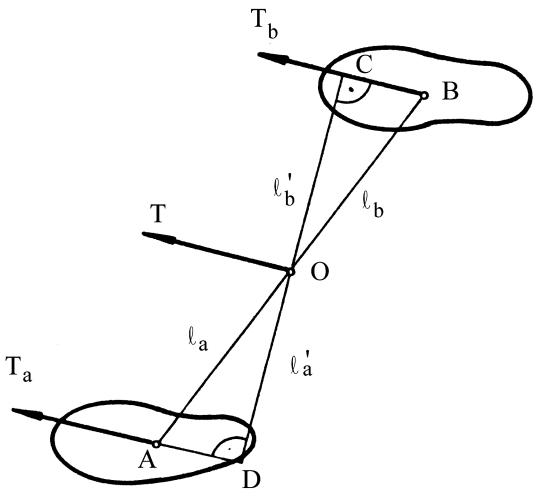

FIGURE 27.8 Determination of total friction force.

where $\vec{F}_{iZ}$ is the projection of $\vec{F}_i$ onto the vertical axis and $\vec{F}_{iX}$ and $\vec{F}_{iY}$ are projections onto the axes X and Y, respectively. Here, the axis Z corresponds to the vertical axis (previously denoted by V) passing through ZMP. The axes X, Y, and Z constitute the absolute orthogonal coordinate frame. Furthermore, the relations $\vec{T} = \vec{T}_a + \vec{T}_b$ and $\vec{R} = \vec{R}_a + \vec{R}_b$ are obvious, and they, together with the relations:

$$\vec{\ell}_a \times \vec{T}_a + \vec{\ell}_b \times \vec{T}_b = 0$$

$$\vec{\ell}_a \times \vec{R}_a + \vec{\ell}_b \times \vec{R}_b = 0 \tag{27.26}$$

extend the possibility of defining the vertical reactions $\vec{R}_a$ and $\vec{R}_b$, as well as the friction forces $\vec{T}_a$ and $\vec{T}_b$. The $\vec{\ell}_a$ and $\vec{\ell}_b$ are the vectors from the ZMP (denoted by 0) to the centers of the corresponding supporting surfaces A and B, respectively.

27.2.3 Biped Dynamics

The active spatial mechanism for realization of the artificial anthropomorphic gait belongs to the class of complex kinematic chains, as shown in Figure 27.9. During walking, the kinematic chain representing the legs changes its configuration from open to closed,[4,13] in the single- and double-support phases, respectively. Each phase involves a different procedure for forming dynamic equations, but it is based on the well-known procedure for dynamic modeling of simple open kinematic chains for robotic manipulators. This procedure enables us to obtain the following expression:[13,14]

$$P = H(q,\theta)\cdot\ddot{q} + h(q,\dot{q},\theta) \tag{27.27}$$

where $P = [P_1, \ldots, P_n]$ is a vector of driving moments at the joints, $H(q,\theta)$ is the $n \times n$ inertial matrix, $h(q,\dot{q},\theta)$ is the $n \times 1$ vector of Coriolis, centrifugal, and gravity forces, $q = [q_1, \ldots, q_n]$ is a vector of joint coordinates, and $\theta = [\theta_1, \ldots, \theta_n]$ is a geometric and dynamic parameter vector.

In the case of complex kinematic chains, the system has at least one link (branching link) belonging to more than two kinematic chains. Calculation of the elements of the matrix H and the vector h of complex kinematic chains can be carried out by introducing the corresponding number

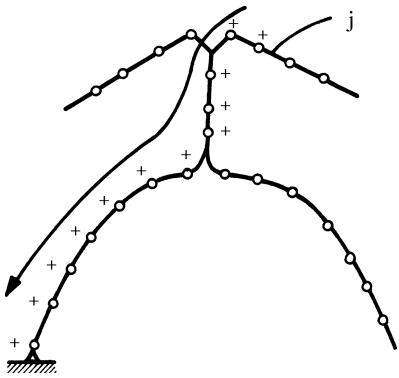

FIGURE 27.9 Complex kinematic chain.

of series of "+" joints.[4,13] A series of "+" joints is formed in such a way that in the case of chain rupture at a certain "+" joint, the *j*-th link should remain in the external part (not connected to the support) of the mechanism. In the course of forming differential equations, the inertial force and moment of the *j*-th mechanism link are reduced to its own "+" joint only, and the following procedure is possible: $\vec{F}_j^u$ and $\vec{M}_j^u$ (total external force and moment) corresponding to the *j*-th link are successively reduced to all "+" joints going from the *j*-th link toward the support. After projecting $\vec{F}_j^u$ and $\vec{M}_j^u$ onto the axis of the *i*-th joint, the resulting quantities denoted by ΔH_{ik}^j and Δh_i^j can be calculated in the following way:[4,13]

$$\Delta H_{ik}^j = -\vec{e}_i\left(\vec{b}_{jk} + \vec{r}_{ji} \times \vec{a}_{jk}\right), \quad \Delta h_i^j = -\vec{e}_i\left(\vec{r}_{ji} \times \left(\vec{a}_j^o + \vec{G}_j\right) + \vec{b}_j^o\right) \tag{27.28}$$

where $\vec{e}_i$ is the unit vector of the *i*-th joint axis, and $\vec{r}_{ji}$ is the radius vector from the *i*-th joint to the *j*-th link center of mass, while $\vec{a}$ and $\vec{b}$ are the corresponding vector coefficients. Note that the angular ($\vec{\varepsilon}_i$) and linear ($\vec{w}_i$) accelerations of the *i*-th link can be expressed as:

$$\vec{\varepsilon}_i = \left[\vec{\alpha}_{i1} \ldots \vec{\alpha}_{ii}\, 0 \ldots 0\right]\ddot{q} + \vec{\alpha}_i^0, \quad \vec{w}_i = \left[\vec{\beta}_{i1} \ldots \vec{\beta}_{ii}\, 0 \ldots 0\right]\ddot{q} + \vec{\beta}_i^0$$

where $\ddot{q} = \left[\ddot{q}^1, \ldots, \ddot{q}^n\right]$. The α_{ij} and β_{ij} are the vector coefficients depending on the generalized coordinates, while the vector coefficients $\vec{\alpha}_i^0$ and $\vec{\beta}_i^0$ depend on the generalized coordinates and velocities. Then, we have:[4,13]

$$\vec{a}_{ij} = -m_i \vec{\beta}_{ij}, \quad \vec{a}_i^0 = -m_i \vec{\beta}_i^0, \quad \vec{b}_{ij} = -T_i \vec{\alpha}_{ij}, \quad \vec{b}_j^0 = -T_i \vec{\alpha}_i^0 + \vec{\lambda}_i$$

with $T_i = \sum_{\ell=1}^{3} Q_{i\ell} J_{i\ell}$, $Q_{i\ell} = \left[q_{i\ell}^1 \vec{q}_{i\ell}^1 \;\; q_{i\ell}^2 \vec{q}_{i\ell}^2 \;\; q_{i\ell}^3 \vec{q}_{i\ell}^3\right]$, and $\vec{\lambda}_i = Q_i \begin{bmatrix} (\vec{\omega}_i \cdot \vec{q}_{i2})(\vec{\omega}_i \cdot \vec{q}_{i3})(J_{i2} - J_{i3}) \\ (\vec{\omega}_i \cdot \vec{q}_{i3})(\vec{\omega}_i \cdot \vec{q}_{i1})(J_{i3} - J_{i1}) \\ (\vec{\omega}_i \cdot \vec{q}_{i1})(\vec{\omega}_i \cdot \vec{q}_{i2})(J_{i1} - J_{i2}) \end{bmatrix}$

where $q_{i\ell}^j$ (j = 1, 2, 3) denotes the *j*-th component of the vector $\vec{q}_{i\ell}$, $\vec{q}_{i\ell}$ denotes the axes of the *i*-th (local) coordinate frame, i.e., the frame attached to the *i*-th link, and J_{ij} is the *j*-th component of the *i*-th link inertia tensor defined with respect to the local coordinate frame associated to each link of the kinematic chain.

The components of matrix *H* and vector *h* are obtained by summing the corresponding values from Equation (27.28) with respect to all series of "+" joints:

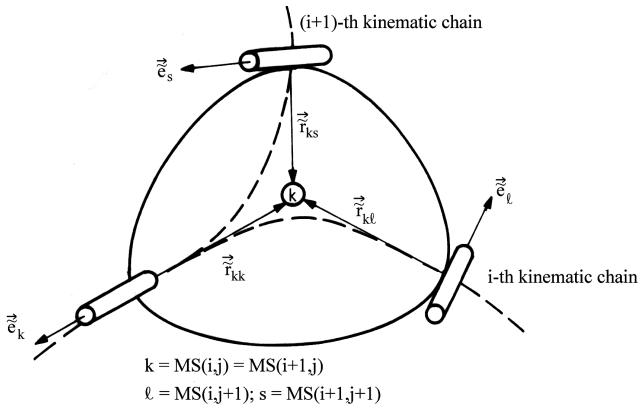

FIGURE 27.10 Branching link of a complex kinematic chain.

$$H_{ik}^{j} = \sum_{(j)} \Delta H_{ik}^{j}, \quad h_i^j = \sum_{(j)} \Delta h_i^j \tag{27.29}$$

Figure 27.10 illustrates a branching link that has three kinematic pairs and is a constituent of two series of "+" joints. The topological structure of the complex chain can be represented by the matrix MS. Each row of this matrix contains ordinal numbers of the corresponding series of "+" joints. The element MS(i,j) is the *j*-th joint in the *i*-th series of "+" joints. In addition, for each series of "+" joints, the ordinal number of the initial joint is also defined. The initial joint of the *i*-th series of "+" joints is the first joint of the *i*-th series differing from joints of the (i–1)-th series of "+" joints. The initial joint of the first series of "+" joints is MS(1,1). For the first link appearing in the first series of "+" joints, the matrix Q_o^o should be known. Q_o^o is a transformation matrix between the reference frame representing ground floor (or basis) and the first link of the kinematic chain resting on the ground floor. It is convenient to place the reference frame just at the contact point. Then, if a fixed support serves as a basis, the matrix Q_o^o is a unit matrix. If we proceed to another chain, then the matrix Q_i^o (Q_i^o is a transformation matrix of the *i*-th link coordinate frame into the reference frame) should be either stored or formed on the basis of the procedure for forming dynamic equations of motion for open kinematic chains. The transformation matrix of the branching link serves to calculate the vectors $\vec{r}$ and $\vec{e}$. Information is needed on the branching link velocities ($\vec{v}$) and accelerations ($\vec{w}$) and the vector coefficients $\vec{\alpha}$, $\vec{\beta}$, $\vec{\alpha}^o$, and $\vec{\beta}^o$.[4,13] All support vectors are equal to zero. These quantities for the mobile branching link should be stored when the preceding chain is analyzed.

To consider the biped dynamics in the double-support phase (Figure 27.11), an equivalent open kinematic chain should be employed. Let us suppose that the terminal link of the equivalent chain does not coincide with the basic link (Figure 27.12). It is possible to determine the translational ($\Delta\vec{\rho}$) and angular ($\Delta\vec{\sigma}$) displacements yielding the coincidence of the two coordinate systems Ψ and Ψ'. Since we consider an open chain equivalent to the closed chain in the dynamic analysis, it is possible to use the same basic procedure as for the open chain.[4,13] Thus, the algorithm should be supplied with an iterative procedure to calculate the position and additional velocities of the first chain. The procedure is repeated until the closure conditions are satisfied.

27.2.4 Example

The nominal dynamics synthesized for the biped locomotion mechanism shown in Figures 27.13 and 27.14 consists of 14 links and 14 revolute joints of the 5-th class for the single-support phase only. Links 5 and 10 are branching links. In the course of motion, the hands are fixed on the chest of the

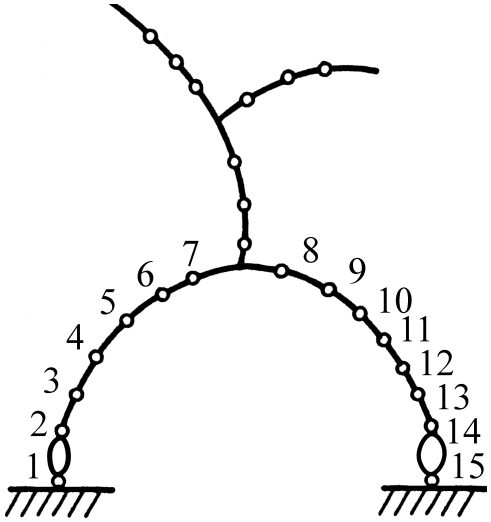

FIGURE 27.11 The anthropomorphic mechanism in double-support position.

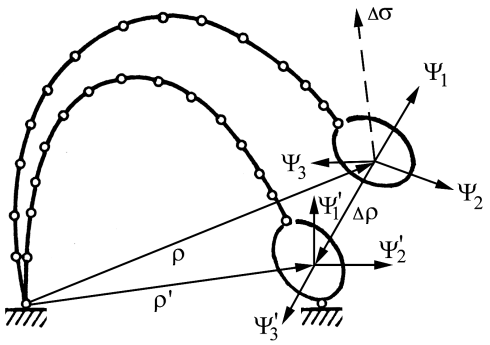

FIGURE 27.12 Terminal link of the equivalent chain.

mechanism. This structure can be split into three kinematic chains containing joints 1 through 8, 9 through 12, and 13 and 14, in the first, second, and third chains, respectively. The topological structure of the complex kinematic chain can be represented by a series of "+" joints in a matrix form:

$$MS = \begin{bmatrix} 1 & 2 & 3 & 4 & 5 & 6 & 7 & 8 & 0 \\ 1 & 2 & 3 & 4 & 5 & 9 & 10 & 11 & 12 \\ 1 & 2 & 3 & 4 & 5 & 9 & 10 & 13 & 14 \end{bmatrix}.$$

Table 27.1 shows numerical values for the mechanical part of the mechanism. The prescribed portion of the mechanism motion is adopted for joints 1 through 8, i.e., for the first chain. This part of the synergy (prescribed synergy) is defined on the basis of the human gait measurements shown in Figure 27.15. A set of prescribed ZMP trajectories for the single-support gait phase is given in Figure 27.16 and the compensation has been synthesized for q^9 and q^{10} (Figure 27.17) to ensure dynamic equilibrium of the mechanism during the motion, in both the sagittal and frontal planes (Figure 27.18).

27.3 Control Synthesis for Biped Gait

Hierarchy is a basic principle on which control of large scale systems is generally based. This holds true for robots as well. The hierarchical organization of the control system is most often vertical, so that each control level deals with wider aspects of the overall system behavior than the lower level.[15-18] A higher control level always refers to the lower ones, and it controls system parameters that vary more slowly. A higher level communicates with a lower level, giving it instructions and receiving from it relevant information required for decision making. After obtaining the information from a lower level, each level makes decisions taking into account decisions obtained from higher levels and forwards them to the lower levels for execution.

27.3.1 Synthesis of Control with Limited Accelerations

Control synthesis is performed in two steps: (a) nominal regimes, and (b) perturbed regimes. For nominal regimes, the control is computed on the basis of the complete (nonlinear) model with the

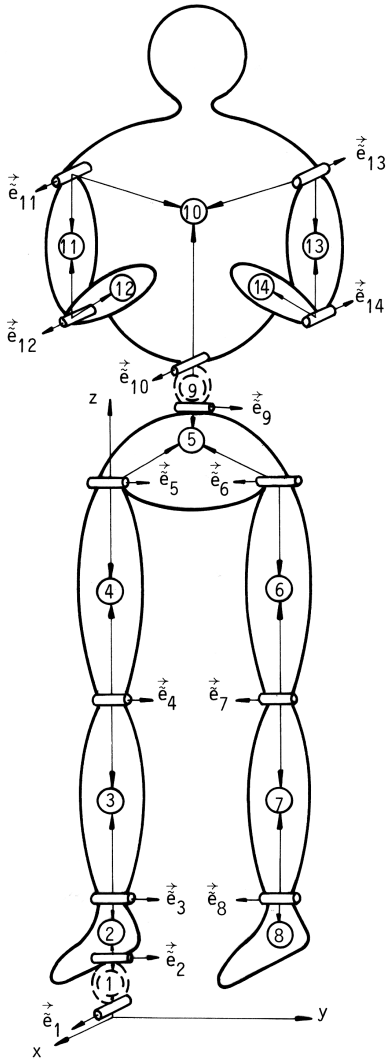

FIGURE 27.13 Mechanical scheme of the anthropomorphic mechanism with fixed arms.

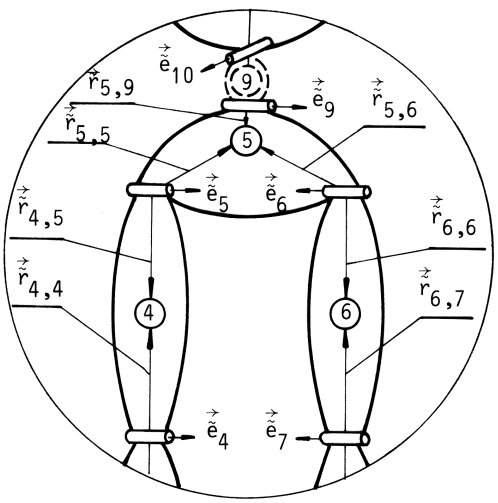

FIGURE 27.14 Notation of $\vec{r}_{i,j}$ vectors.

permanent requirement of satisfying dynamic equilibrium conditions for the overall mechanism. This control should enable the system (in the absence of disturbance) to follow the nominal trajectories. For perturbed regimes, the control should force the state vector to its nominal value, i.e., to the nominal programmed trajectory. The action should be smooth, with no significant change in link acceleration, to keep its influence on the unpowered DOFs within an acceptable range.[13,19] Let us consider the overall system model defined as:

$$S^i:\ \dot{x} = \hat{A}(x) + \hat{B}(x)N(u)$$

Assume that the part of the system corresponding to powered DOFs can be rearranged as a set of subsystems S_a^i coupled via the term $\left(f_c^i \cdot P_c^i\right)$:

$$S_a^i:\quad \dot{x}_c^i = A_c^i x_c^i + b_c^i N(u^i) + f_c^i P_c^i\,,\quad \forall i \in I_1$$

TABLE 27.1 Kinematic and Dynamic Parameters of the Mechanism

Link	Mass (kg)	Moment of Inertia (kgm²) J_X	J_Y	J_Z	Distance of the Axes Centers of Joints from the Link Center (m)	Joint Unit Axes
1	0.0	0.0	0.0	0.0	$\vec{\tilde{r}}_{1,1} = (0,0,0.0001)^T$; $\vec{\tilde{r}}_{1,2} = (0,0,-0.0001)^T$	$\vec{\tilde{e}}_1 = (1,0,0)^T$
2	1.53	0.00006	0.00055	0.00045	$\vec{\tilde{r}}_{2,2} = (0,0,0.030)^T$; $\vec{\tilde{r}}_{2,3} = (0,0,-0.070)^T$	$\vec{\tilde{e}}_2 = (0,1,0)^T$
3	3.21	0.00393	0.00393	0.00038	$\vec{\tilde{r}}_{3,3} = (0,0,0.210)^T$; $\vec{\tilde{r}}_{3,4} = (0,0,-0.210)^T$	$\vec{\tilde{e}}_3 = (0,1,0)^T$
4	8.41	0.01120	0.01200	0.00300	$\vec{\tilde{r}}_{4,4} = (0,0,0.220)^T$; $\vec{\tilde{r}}_{4,5} = (0,0,-0.220)^T$	$\vec{\tilde{e}}_4 = (0,1,0)^T$
5	6.96	0.00700	0.00565	0.00627	$\vec{\tilde{r}}_{5,5} = (0,0.135,0.1)^T$; $\vec{\tilde{r}}_{5,6} = (0,-0.135,0.1)^T$; $\vec{\tilde{r}}_{5,9} = (0,0,-0.05)^T$	$\vec{\tilde{e}}_5 = (0,1,0)^T$
6	8.41	0.01120	0.01200	0.00300	$\vec{\tilde{r}}_{6,6} = (0,0,-0.220)^T$; $\vec{\tilde{r}}_{6,7} = (0,0,0.220)^T$;	$\vec{\tilde{e}}_6 = (0,-1,0)^T$
7	3.21	0.00393	0.00393	0.00038	$\vec{\tilde{r}}_{7,7} = (0,0,-0.210)^T$; $\vec{\tilde{r}}_{7,8} = (0,0,0.210)^T$	$\vec{\tilde{e}}_7 = (0,-1,0)^T$
8	1.53	0.00006	0.00055	0.00045	$\vec{\tilde{r}}_{8,8} = (0,0,-0.070)^T$	$\vec{\tilde{e}}_8 = (0,-1,0)^T$
9	0.0	0.0	0.0	0.0	$\vec{\tilde{r}}_{9,9} = (0,0,0.0001)^T$; $\vec{\tilde{r}}_{9,10} = (0,0,-0.0001)^T$	$\vec{\tilde{e}}_9 = (0,1,0)^T$
10	30.85	0.15140	0.13700	0.02830	$\vec{\tilde{r}}_{10,10} = (0,0,0.34)^T$; $\vec{\tilde{r}}_{10,11} = (0,0.2,-0.06)^T$; $\vec{\tilde{r}}_{10,13} = (0,-0.2,-0.06)^T$	$\vec{\tilde{e}}_{10} = (1,0,0)^T$
11	2.07	0.00200	0.00200	0.00022	$\vec{\tilde{r}}_{11,11} = (0,0,-0.154)^T$; $\vec{\tilde{r}}_{11,12} = (0,0,0.154)^T$	$\vec{\tilde{e}}_{11} = (1,0,0)^T$
12	1.14	0.00250	0.00425	0.00014	$\vec{\tilde{r}}_{12,12} = (0,0,-0.132)^T$	$\vec{\tilde{e}}_{12} = (1,0,0)^T$
13	2.07	0.00200	0.00200	0.00022	$\vec{\tilde{r}}_{13,13} = (0,0,-0.154)^T$; $\vec{\tilde{r}}_{13,14} = (0,0,0.154)^T$	$\vec{\tilde{e}}_{13} = (-1,0,0)^T$
14	1.14	0.00250	0.00425	0.00014	$\vec{\tilde{r}}_{14,14} = (0,0,-0.132)^T$	$\vec{\tilde{e}}_{14} = (-1,0,0)^T$

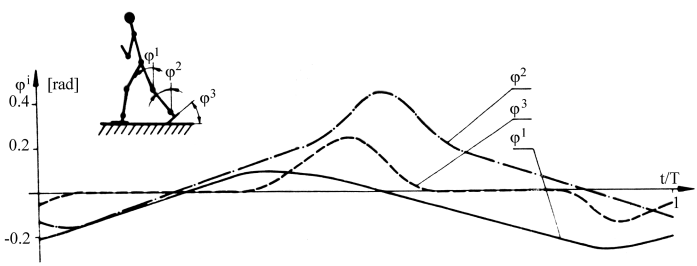

FIGURE 27.15 Synergy for walking upon level ground.

where $A_c^i \in R^{n_i x n_i}$ is the subsystem matrix, whereas $b_c^i \in R^{n_i}$ and $f_c^i \in R^{n_i}$ are distribution vectors of the input control signal and force, respectively, $x_c^i \in R^{n_i}$ is the subsystem state vector, $u^i \in R^1$ and $P_c^i \in R^1$ are the scalar values of control input and generalized force of the i-th subsystem, $i \in I_1$, $I_1 = \{i, i = 1,2,...,m\}$, $N(u^i)$ is the nonlinearity of the amplitude saturation type.

Let the nominal trajectory x_c^o, $x_c^o = \left(x_c^{o1^T}, x_c^{o2^T}, \ldots, x_c^{om^T}\right)^T$ and the nominal control u^o, $u^o = \left(u^{o1}, u^{o2}, ..., u^{om}\right)^T$ be introduced in such a way to satisfy:

$$S_a^i: \quad \dot{x}_c^{oi} = A_c^i x_c^{oi} + b_c^i N(u^{oi}) + f_c^i P_c^{oi}, \quad \forall i \in I_1. \tag{27.30}$$

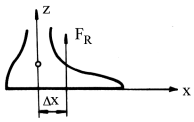

ZMP displacement

CASE	t(sec)	Δx (m)
I	0 ÷ T/2	0.0
II	0 ÷ 0.3 0.3 ÷ T/2	0.0 0.035
III	0 ÷ 0.5 0.5 ÷ T/2	0.0 0.035
IV	0 ÷ 0.2 0.2 ÷ 1.0 1.0 ÷ T/2	-0.02 0.0 0.0
V	0 ÷ 0.2 0.2 ÷ 0.6 0.6 ÷ T/2	-0.02 0.0 0.035

FIGURE 27.16 Set of ZMP trajectories for the single-support gait phase.

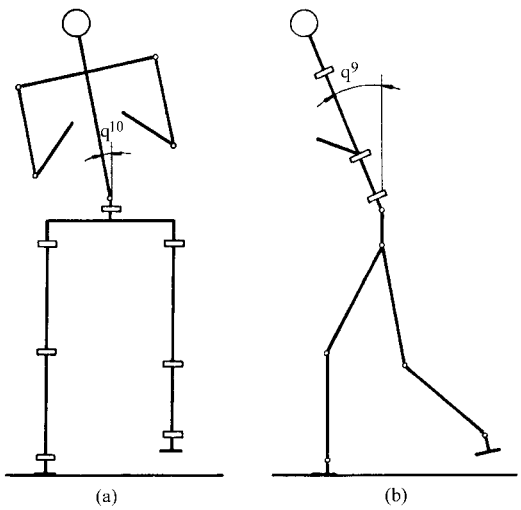

FIGURE 27.17 Compensating DOF in the frontal (a) and sagittal (b) planes.

Then, the model of subsystem deviation from the nominal is considered in the form:

$$\Delta\dot{x}_c^i = A_c^i \Delta x_c^i + b_c^i N(\Delta u^i) + f_c^i \Delta P_c^i, \quad \forall i \in I_1 . \tag{27.31}$$

The purpose of the synthesis of disturbance-compensating control (Δu) is to force the system deviation Δx_c^i, (i = 1, 2, …, m) to zero, to maintain the overall system dynamic balance.

We shall synthesize the local controller for the *i*-th actuator, i.e., for the S_a^i subsystem whose model of state deviation around the nominal trajectory is given by Equation (27.31). We want to define the controller for this subsystem that will reduce the state deviation $\Delta x_c^i(t)$ to zero, but in doing so we want to prevent the appearance of very high accelerations. Therefore, we shall synthesize a controller that will ensure the acceleration of the corresponding joint $\Delta\ddot{q}^i$ be limited. We start with the simple problem of the second order linear system with limited accelerations.[13,19]

Let us consider the classical time-minimum problem. Let the system be described by:

$$\Delta\dot{q}_1^i(t) = \Delta q_2^i(t)$$

$$\Delta\dot{q}_2^i(t) = u_i^*(t) \quad \left|u_i^*(t)\right| \le \Omega^i \tag{27.32}$$

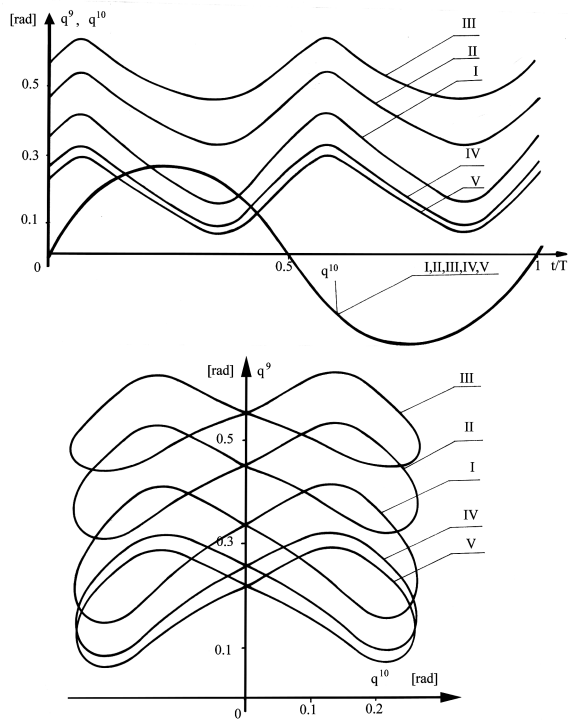

FIGURE 27.18 Compensating movements for the single-support gait upon level ground for T = 1.5, S = 0.6, and ZMP laws from Figure 27.16.

with the initial conditions $\Delta q_1^i(0)=\alpha^i$ and $\Delta q_2^i(0)=\beta^i$, where $\Omega^i \in R^1$, $\Delta q_1^i \in R^1$, and $\Delta q_2^i \in R^1$. The value $u_i^*(t)$ should be computed in such a way to ensure that the system (27.32) returns from $\left(\alpha^i, \beta^i\right)$ to the point (0, 0) in a minimal time interval.

Therefore, such a solution of Equation (27.32) should be obtained that the functional $J=\int_0^{T^*} dt$ is at minimum, where $T^* \in R^1$ defines an unspecified time interval. Such types of problems are well known, and for this particular case ($\Omega^i \neq 1$), its solution is given by the expression:

$$u_i^*=\begin{cases} +\Omega^i \quad \text{if} \quad \Delta q_1^i < \dfrac{\Delta q_2^i \left|\Delta q_2^i\right|}{2\Omega^i} \quad \text{or} \quad \Delta q_1^i = \dfrac{\left(\Delta q_2^i\right)^2}{2\Omega^i} \wedge \Delta q_2^i \leq 0 \\ -\Omega^i \quad \text{if} \quad \Delta q_1^i > \dfrac{-\Delta q_2^i \left|\Delta q_2^i\right|}{2\Omega^i} \quad \text{or} \quad \Delta q_1^i = \dfrac{-\left(\Delta q_2^i\right)^2}{2\Omega^i} \wedge \Delta q_2^i \geq 0 \end{cases} . \tag{27.33}$$

We shall apply this solution to control one single actuator, i.e., the subsystem S_a^i associated with the *i*-th joint. Let us suppose the mechanism is powered by DC motors whose models are given in the form (the state vector $\Delta x_c^i=(\Delta q^i, \Delta \dot{q}^i, \Delta i_R^i)^T$:

$$\begin{bmatrix} \Delta \dot{q}^i \\ \Delta \ddot{q}^i \\ \Delta \dot{i}_R^i \end{bmatrix} = \begin{bmatrix} 0 & 1 & 0 \\ 0 & a_{22}^i & a_{23}^i \\ 0 & a_{32}^i & a_{33}^i \end{bmatrix} \begin{bmatrix} \Delta q^i \\ \Delta \dot{q}^i \\ \Delta i_R^i \end{bmatrix} + \begin{bmatrix} 0 \\ \bar{f}_c^i \\ 0 \end{bmatrix} \Delta P_c^{i*} + \begin{bmatrix} 0 \\ 0 \\ \bar{b}_c^i \end{bmatrix} \Delta u^i . \tag{27.34}$$

From the second equation of (27.34) we can write:

$$\Delta i_R^{i*} = (u^{i*} - a_{22}^i \, \Delta \dot{q}^i - \bar{f}_c^i \, \Delta P_c^i) / a_{23}^i \tag{27.35}$$

where $\Delta \ddot{q}^i$ is replaced by the value of the allowed link acceleration u^{i*} from (27.33). Then, Δi_R^{i*} in (27.35) is the corresponding rotor current, and its derivative can be computed from the following expression:

$$\Delta \dot{i}_R^i = \left(\Delta i_R^{i*} - \Delta i_R^i\right) / \Delta t \tag{27.36}$$

where $\Delta t \in R^1$ is the control sampling period. Now we can determine the control for Equation (27.34). Let us assume that we want to limit acceleration of the actuator (joint) within the limits $\Omega_{\min}^i$ and $\Omega_{\max}^i$. Starting from the time-minimum control (Equation (27.33)) we can adopt the following control. From the third equation of Equation (27.34) the compensation control signal for the i-th actuator is[13]

$$\Delta u^i = k_{i1}^L \Delta q^i + k_{i2}^L \Delta \dot{q}^i + k_{i3}^L \Delta \dot{i}_R^i + k_{i4}^G \Delta P_c^{i*} + k_{i5}^G \tag{27.37}$$

where the constant feedback gains are

$$k_{i1}^L = 0, \quad k_{i2}^L = \left(-a_{22}^i - a_{23}^i \cdot a_{32}^i \cdot \Delta t\right) / d$$

$$k_{i3}^L = -a_{23}^i \left(1 + a_{33}^i \cdot \Delta t\right) / d, \quad k_{i4}^G = -\bar{f}_c^i / d, \quad k_{i5}^G = k_{i5} / d \tag{27.38}$$

$$k_i^5 = \begin{cases} \Omega_{\max}^i & \text{if} \quad \Delta q^i < \dfrac{-0.5 \Delta \dot{q}^i \left|\Delta \dot{q}^i\right|}{\Omega^i} \quad \text{or} \quad \Delta q^i = \dfrac{0.5 \left(\Delta \dot{q}^i\right)^2}{\Omega^i} \ \wedge \ \Delta \dot{q}^i < 0 \\ \Omega_{\min}^i & \text{if} \quad \Delta q^i > \dfrac{-0.5 \Delta \dot{q}^i \left|\Delta \dot{q}^i\right|}{\Omega^i} \quad \text{or} \quad \Delta q^i = \dfrac{-0.5 \left(\Delta \dot{q}^i\right)^2}{\Omega^i} \ \wedge \ \Delta \dot{q}^i > 0 \end{cases}$$

where $d = a_{23}^i \bar{b}_c^i \Delta t$, a_{jk}^i, $\bar{b}_c^i$, $\bar{f}_c^i$ are the elements of the corresponding matrix and vectors of the actuator (27.34), $\Omega_{\max}^i$ and $\Omega_{\min}^i$ are the maximal and minimal values of the accelerations of the i-th link. The feedback gains synthesized in this way have to ensure compensating movements such that the accelerations do not exceed a certain predetermined limit. As a consequence, the induced inertial forces will not cause an undesirable motion of the unpowered DOFs, i.e., the displacement of ZMP out of a prescribed area. The proposed control law (27.37) consists of two parts: local control and global control (concerning feedback with respect to ΔP_c^{i*} from the rest of the system upon the i-th subsystem). The term k_{i5}^G may be conditionally associated with global control, although it is based upon local feedback information. The global control ($k_{i4}^G \Delta P_c^{i*}$) requires information on the coupling acting upon the i-th subsystem.

27.3.2 Synthesis of Global Control with Respect to ZMP Position

The decentralized control defined by Equation (27.37) applied at the mechanism's joints is not sufficient to ensure tracking of internal nominal trajectories with the addition of the appropriate behavior of the unpowered subsystem. An additional feedback must be introduced at one of the powered joints to ensure satisfactory motion of the complete mechanism. The task of this feedback is to reduce the destabilizing effect of the coupling acting upon the unpowered subsystems.

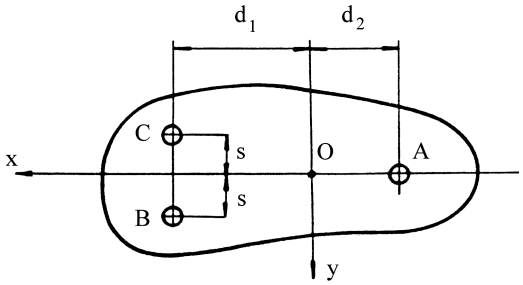

FIGURE 27.19 Disposition of the force sensors on the mechanism sole.

Since a dominant role in system stability is played by the unpowered DOFs it is necessary to reduce the destabilizing coupling effects acting upon them. Because the unpowered subsystem cannot compensate for its own deviation from the nominal state, one of the powered subsystems has to be chosen to accomplish it. As coupling of the subsystems S^j is a function of control input to the i-th subsystem S_a^i, it is clear that a feedback from the subsystem S^j to the inputs Δu^i of the subsystem S_a^i should be introduced.

In dealing with bipeds,[13,20] where the unpowered DOFs are formed by contact of the feet and the ground, it is possible to measure the ground reaction force with the aid of force sensors (at least three) to determine the acting point of total vertical reaction force. For the known motion of the overall mechanism, the ground reaction force (or force in double-support phase) is defined by the intensity, direction, and position of the acting point on the foot. If force sensors A, B, and C are introduced (Figure 27.19) and the system is performing gait, the measured values of vertical reaction forces R_A, R_B, and R_C correspond to their nominal values, and the nominal position of ZMP can be determined. Measurement of the vertical reaction forces R_A, R_B, and R_C when the mechanism is performing gait in the presence of disturbances enables the determination of the actual position of ZMP. If the nominal ZMP position corresponds to point 0, it can be written:

$$s(\Delta R_B - \Delta R_C) = M_x = R_z \cdot \Delta y$$

$$d_1(\Delta R_B + \Delta R_C) - d_2 \Delta R_A = M_y = R_z \cdot \Delta x \tag{27.39}$$

where ΔR_A, ΔR_B, and ΔR_C are the deviations of the corresponding measured forces from their nominal values, R_z is the total vertical reaction force, and Δx and Δy are the displacements of ZMP from its nominal position. These displacements can be computed from Equation (27.39), provided the sensor dispositions and vertical reaction forces are known. The actual position of the ZMP is the best indicator of overall biped behavior, and we can use it to achieve a dynamically balanced motion. Our aim is to synthesize such control that will ensure a stable gait. The primary task of the feedback with respect to ZMP position is to prevent its excursion out of the allowable region, i.e., to prevent the system from falling by rotation about the foot edge. If this is fulfilled, a further requirement imposed is to ensure that the actual ZMP position is as close as possible to the nominal.

Our further discussion will be limited to biped motion in the sagittal plane, which means that the ground reaction force position will deviate only in the direction of the x axis by Δx. Figure 27.20 illustrates the case when the vertical ground reaction force R_z deviates from the nominal position 0 by Δx; thus, the moment $R_z \cdot \Delta x = M_{ZMP}^x$ is a measure of the mechanism's overall behavior.

In the same way we can consider the mechanism motion in the frontal plane. $R_z \cdot \Delta y = M_{ZMP}^y$ is a measure of the mechanism's behavior in the direction of the y axis. Let us assume the correction of the R_z acting point in one direction is done by the action at only one joint, arbitrarily selected in advance. A basic assumption introduced for the purpose of simplicity is that the action at the chosen joint will not cause a change in the motion at any other joint. If we consider only this

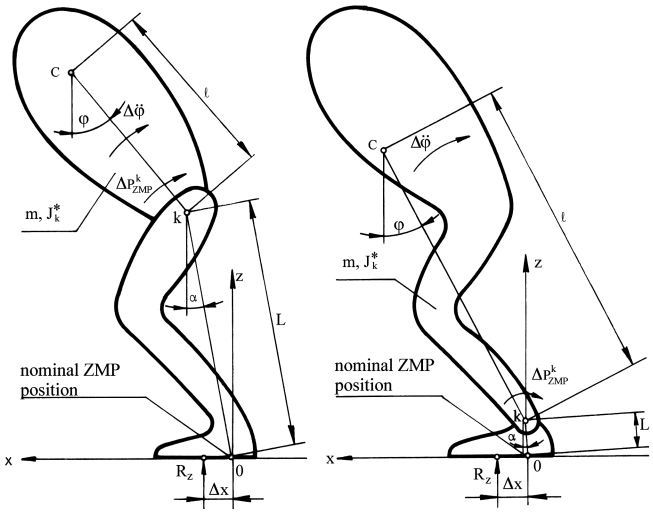

FIGURE 27.20 Compensation of ZMP displacement by (a) hip joint, and (b) ankle joint.

action, the system will behave as if composed of two rigid links connected at the joint *k,* as presented in Figure 27.20. In other words, the servo systems are supposed to be sufficiently stiff. In Figure 27.20, two situations are illustrated: (case a) when the hip of the supporting leg is the joint compensating for the ZMP displacement, and (case b) when the ankle joint is that joint. In both cases, this joint is denoted by *k,* and all links above and below it are considered as a single rigid body. The upper link is of the total mass *m* and inertia moment J_k^* for the axis of the joint *k*. Of course, numerical values are different for both cases.

The distance from the ground surface to *k* is denoted by L, from *k* to C (mass center of the upper link) by ℓ, whereas ΔP_{ZMP}^k stands for the additional correctional torque applied to the joint *k.* In Figure 27.20, the upper (compensating) link is presented as a single link above the joint *k*. In both cases presented, the compensating link includes the other leg (not drawn in the figure), which is in the swing phase. The calculation of the inertia moment J_k^* must include all the links found further onward with respect to the selected compensating joint. All the joints except the *k*-th joint are considered frozen, and, as a consequence, the lower link, representing the sum of all the links below the *k*-th joint, is considered a rigid body standing on the ground surface and performing no motion.

The procedure by which the correctional amount of global control is synthesized with respect to ZMP position is as follows. Assume the mechanism performs the gait such that displacement of the ground reaction force $\vec{R}$ in the *x* direction occurs, so $M_{ZMP}^x = R_z \cdot \Delta x$. The quantity ΔP_{ZMP}^k is to be determined on the basis of the value M_{ZMP}^x and the known mechanism and gait characteristics. Assume that the additional torque ΔP_{ZMP}^k will cause change in acceleration of the compensating link $\Delta\ddot{\varphi}$, while velocities will not change due to the action of ΔP_{ZMP}^k, $\Delta\dot{\varphi} \approx 0$. From the equation of planar motion of the considered system of two rigid bodies (Figure 27.20), which is driven by ΔP_{ZMP}^k, and under the assumption that the terms $(\dot{\varphi}\,\Delta\dot{\varphi})$ and $(\Delta\dot{\varphi})^2$ in the expression for normal component of angular acceleration of the upper link are neglected, it follows that:[13,19]

$$\Delta P_{ZMP}^k = \frac{M_{ZMP}^x}{1 + \dfrac{m \cdot \ell \cdot L \cdot \cos\varphi\,\cos\alpha}{J_k^*} + \dfrac{m \cdot \ell \cdot L \cdot \sin\varphi\,\sin\alpha}{J_k^*}}. \tag{27.40}$$

The control input to the actuator of the compensating joint that has to realize ΔP_{ZMP}^k can be computed from the model of the actuator deviation from the nominal. Thus:

$$\begin{bmatrix} \Delta\dot{q}^k \\ \Delta\ddot{q}_T^k \\ \Delta\dot{i}_R^k \end{bmatrix} = \begin{bmatrix} 0 & 1 & 0 \\ 0 & a_{22}^k & a_{23}^k \\ 0 & a_{32}^k & a_{33}^k \end{bmatrix} \begin{bmatrix} \Delta q^k \\ \Delta\dot{q}^k \\ \Delta i_R^k \end{bmatrix} + \begin{bmatrix} 0 \\ \bar{f}_c^k \\ 0 \end{bmatrix} (\Delta P_c^k + \Delta P_{ZMP}^k) + \begin{bmatrix} 0 \\ 0 \\ \bar{b}_c^k \end{bmatrix} (\Delta u^k + \Delta u_{ZMP}^k). \quad (27.41)$$

This model differs from Equation (27.34) by the terms ΔP_{ZMP}^k and Δu_{ZMP}^k. From the second equation of (27.41), the change of the rotor current is:

$$\Delta i_R^k = \frac{\Delta\ddot{q}_T^k - a_{22}^k \cdot \Delta\dot{q}^k - \bar{f}_c^k (\Delta P_c^k + \Delta P_{ZMP}^k)}{a_{23}^k}. \quad (27.42)$$

Here the subscript T is used for the acceleration $\Delta\ddot{q}^k$ from Equation (27.41). It denotes the total change of link acceleration, which consists of two parts. The first part is the regular change of acceleration due to the control already applied to each powered joint defined by Equation (27.37) and corresponds to ΔP_c^k. The second part is a direct consequence of the compensation torque ΔP_{ZMP}^k. Thus:

$$\Delta\ddot{q}_T^k \approx \Delta\ddot{q}^k + \Delta\ddot{q}_{ZMP}^k \approx \Delta\ddot{q}^k + \frac{\Delta P_{ZMP}^k}{J_k^*} \quad (27.43)$$

where $\Delta\ddot{q}^k(t) \approx (\Delta\dot{q}^k(t) - \Delta\dot{q}^k(t-\Delta t)/\Delta t$. Then, from the third equation of (27.41) we have:

$$\Delta u_{ZMP}^k = \frac{\Delta\dot{i}_R^k - a_{32}^k \cdot \Delta\dot{q}^k - a_{33}^k \cdot \Delta i_R^k}{\bar{b}_c^k} - \Delta u^k \quad (27.44)$$

where Δu^k is the control defined by Equation (27.37), while $\Delta\dot{i}_R^k$ stands for $\Delta\dot{i}_R^k(t) \approx (\Delta i_R^k(t) - \Delta i_R^k(t+\Delta t))/\Delta t$. Equation (27.44) defines the control input to the k-th actuator that has to produce ΔP_{ZMP}^k. Taking into account that ΔP_{ZMP}^k is derived by introducing certain simplifications, an additional feedback gain $k_{ZMP}^{Gk} \in R^1$ has to be introduced into Equation (27.44). Thus, Equation (27.44) becomes:

$$\Delta u_{ZMP}^k = k_{ZMP}^{Gk} \left(\frac{\Delta\dot{i}_R^k - a_{32}^k \cdot \Delta\dot{q}^k - a_{33}^k \cdot \Delta i_R^k}{\bar{b}_c^k} - \Delta u^k \right) \quad (27.45)$$

The additional feedback and correctional input to the selected powered mechanism's subsystem have the purpose only of maintaining the ZMP position. It is quite possible that the feedback introduced could spoil the tracking of the internal nominal trajectory of the joint k, but the dynamic stability of the overall system would be preserved, which is the most important goal of a locomotion system. Which of the joints (ankle, hip, etc.) is most suitable for this purpose cannot be determined in advance, because the answer depends on the task imposed. In Figure 27.21 a scheme of the control is given with feedback introduced with respect to the ZMP position.

27.3.3 Example

The scheme of the biped structure used for the gait simulation is presented in Figure 27.22 and its mechanical parameters are given in Table 27.2. The joint with more than one DOF has been modeled as a set of corresponding numbers of simple rotational joints connected with light links of zero length ($\vec{r}_{i,k} = 0$). These are called fictitious links, and in Figure 27.22 are represented by a dashed

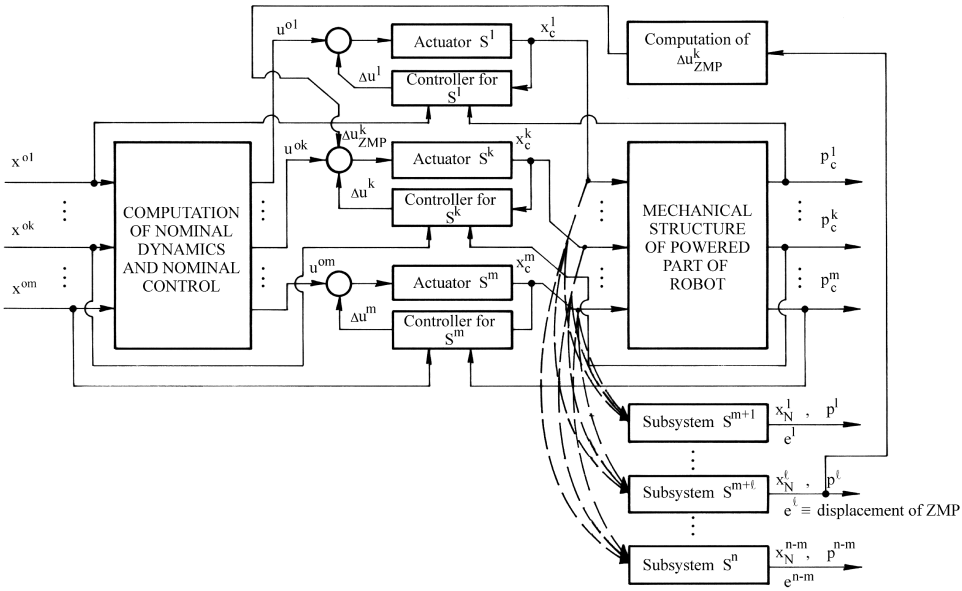

FIGURE 27.21 Control scheme with global feedback from the *l*-th unpowered subsystem to the *k*-th powered subsystem.

line. For example, simple rotational joints with the unit rotational axes $\vec{e}_3$ and $\vec{e}_4$ connected to the fictitious link 3 constitute the ankle joint of the right leg. In a similar way we can represent the hip and trunk joints. Other joints possess one DOF only.[13]

Since the mechanism in the single-support phase can rotate as a whole about the foot edges in the frontal and sagittal planes, these two DOFs are modeled as simple rotational joints with the axes $\vec{e}_1$ and $\vec{e}_2$ below the supporting foot. The mechanism rotation about the z axis is supposed to be prevented by sufficiently large friction between the sole mechanism and the ground surface. The nominal motion is synthesized using the prescribed synergy method. The compensating movements are executed by the trunk in the sagittal and frontal planes about $\vec{e}_{15}$ and $\vec{e}_{16}$.

The motion is simulated for one half-step period and for the single-support phase only. Duration time of the simulated motion was T = 0.75 s. The perturbed motion of the system around the nominal trajectory was simulated, and the trunk angular displacement from the nominal trajectory in the sagittal plane of $\Delta q^{15}(0) = 0.2\ [rad]$ was adopted as disturbance at the initial moment. Each gait is simulated using three different values of $\Omega^i_{\max}$ (i = 4 for the ankle joint, i = 15 for the trunk) defined by k^G_{i5}. They are $|\Omega^i_{\max}| = 3[rad/s^2]$, $|\Omega^i_{\max}| = 5[rad/s^2]$, and $|\Omega^i_{\max}| = 7[rad/s^2]$. Figure 27.23 presents the case when only local feedback gains defined by Equation (27.38) are employed but without feedback with respect to the overall system equilibrium. The trunk deviation Δq^{15} converges to the nominal value, but the deviations Δq^4 (ankle joint) and Δq^6 (hip joint) slightly diverge — the absolute values of these deviations are, however, very small.

Figure 27.24 gives the example of ZMP displacement compensated by the ankle joint. Again, the trunk inclination for 0.2 [rad] was adopted as initial disturbance and $k^{Gk}_{ZMP} = 0.5$. Figure 27.24e illustrates the ZMP behavior; maximal average deviation is about 1 cm, which can be considered very successful. Behavior of the other joints, especially of the ankle, is not affected much by keeping ZMP position strongly under control.

27.4 Dynamic Stability Analysis of Biped Gait

The system is considered a set of subsystems, each of which is associated with one powered joint. The stability of each subsystem is checked (neglecting the coupling) and then dynamic coupling

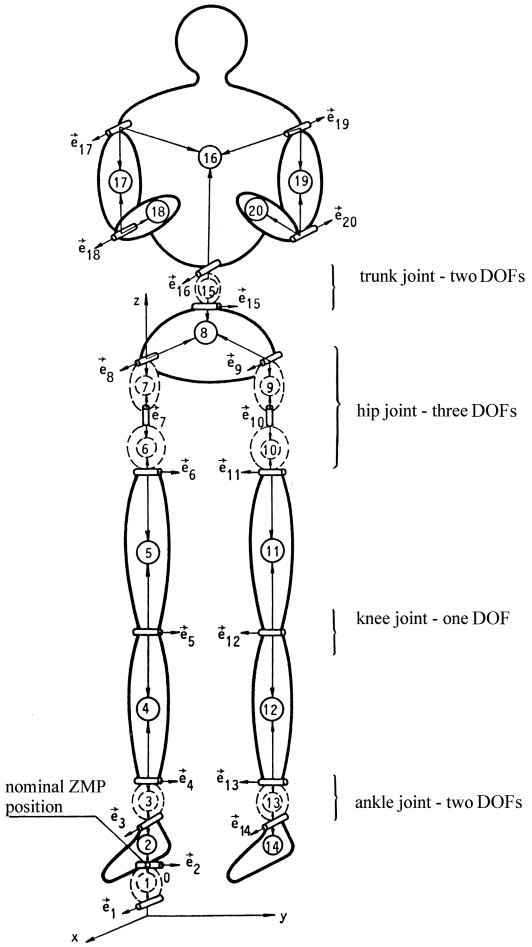

FIGURE 27.22 Scheme of mechanical biped structure.

between the subsystems is analyzed. The stability of the overall system is tested by taking into account all dynamic interconnections between the subsystems. However, these tests require that all subsystems are stable. To analyze stability of the mechanisms including unpowered joints, we introduced the so-called composite subsystems that consist of one powered and one unpowered joint. Thus we obtain a subsystem which, if considered decoupled from the rest of the system, might be stabilized. Further, the interconnections of the composite subsystem with the rest of subsystems are taken into account, and a test for stability of the overall mechanism is established.

To analyze stability of the locomotion mechanisms, we shall use the aggregation– decomposition method via Lyapunov vector functions in bounded regions of state space, originally developed for manipulation robots.[13,21,22] Since it is valid for the mechanism with all joints powered, this method cannot be directly applied to locomotion mechanisms containing unpowered DOFs. Because of that, we modified the subsystem modeling by incorporating the models of unpowered DOFs into the composite subsystem models. In this way, the entire mechanism is considered in the stability analysis.[13,22]

27.4.1 Modeling of Composite Subsystems

The mathematical model of the complete system S consists of two parts: the model of mechanical structure S^M and the model of actuators S_a^i. These models are:[13,17]

TABLE 27.2 Kinematic and Dynamic Parameters of the Mechanism

Link	Mass (kg)	Moment of Inertia (kgm²)			Distance of the Axes Centers of Joints from the Link Center (m)	Joint Unit Axes
		J_X	J_Y	J_Z		
1	0.0	0.0	0.0	0.0	$\vec{\tilde{r}}_{1,1} = (0,0,0.0001)^T$; $\vec{\tilde{r}}_{1,2} = (0,0,-0.0001)^T$	$\vec{\tilde{e}}_1 = (1,0,0)^T$
2	1.53	0.00006	0.00055	0.00045	$\vec{\tilde{r}}_{2,2} = (0,0,0.030)^T$; $\vec{\tilde{r}}_{2,3} = (0,0,-0.070)^T$	$\vec{\tilde{e}}_2 = (0,1,0)^T$
3	0.0	0.0	0.0	0.0	$\vec{\tilde{r}}_{3,3} = (0,0,0.0001)^T$; $\vec{\tilde{r}}_{3,4} = (0,0,-0.0001)^T$	$\vec{\tilde{e}}_3 = (1,0,0)^T$
4	3.21	0.00393	0.00393	0.00038	$\vec{\tilde{r}}_{4,4} = (0,0,0.210)^T$; $\vec{\tilde{r}}_{4,5} = (0,0,-0.210)^T$	$\vec{\tilde{e}}_4 = (0,1,0)^T$
5	8.41	0.01120	0.01200	0.00300	$\vec{\tilde{r}}_{5,5} = (0,0,0.220)^T$; $\vec{\tilde{r}}_{5,6} = (0,0,-0.220)^T$	$\vec{\tilde{e}}_5 = (0,1,0)^T$
6	0.0	0.0	0.0	0.0	$\vec{\tilde{r}}_{6,6} = (0,0,0.0001)^T$; $\vec{\tilde{r}}_{6,7} = (0,0,-0.0001)^T$;	$\vec{\tilde{e}}_6 = (0,1,0)^T$
7	0.0	0.0	0.0	0.0	$\vec{\tilde{r}}_{7,7} = (0,0,0.0001)^T$; $\vec{\tilde{r}}_{7,8} = (0,0,-0.0001)^T$	$\vec{\tilde{e}}_7 = (1,0,0)^T$
8	6.96	0.00700	0.00565	0.00625	$\vec{\tilde{r}}_{8,8} = (0,0.135,0.1)^T$; $\vec{\tilde{r}}_{8,9} = (0,-0.135,0.1)^T$; $\vec{\tilde{r}}_{8,15} = (0,0,-0.05)^T$	$\vec{\tilde{e}}_8 = (1,0,0)^T$
9	0.0	0.0	0.0	0.0	$\vec{\tilde{r}}_{9,9} = (0,0,-0.0001)^T$; $\vec{\tilde{r}}_{9,10} = (0,0,0.0001)^T$	$\vec{\tilde{e}}_9 = (1,0,0)^T$
10	0.0	0.0	0.0	0.0	$\vec{\tilde{r}}_{10,10} = (0,0,-0.0001)^T$; $\vec{\tilde{r}}_{10,11} = (0,0,0.0001)^T$;	$\vec{\tilde{e}}_{10} = (0,0,1)^T$
11	8.41	0.01120	0.01200	0.00300	$\vec{\tilde{r}}_{11,11} = (0,0,-0.220)^T$; $\vec{\tilde{r}}_{11,12} = (0,0,0.220)^T$	$\vec{\tilde{e}}_{11} = (0,-1,0)^T$
12	3.21	0.00393	0.00393	0.00038	$\vec{\tilde{r}}_{12,12} = (0,0,-0.210)^T$; $\vec{\tilde{r}}_{12,13} = (0,0,0.210)^T$	$\vec{\tilde{e}}_{12} = (0,-1,0)^T$
13	0.0	0.0	0.0	0.0	$\vec{\tilde{r}}_{13,13} = (0,0,-0.0001)^T$; $\vec{\tilde{r}}_{13,14} = (0,0,0.0001)^T$	$\vec{\tilde{e}}_{13} = (0,-1,0)^T$
14	1.53	0.00006	0.00055	0.00045	$\vec{\tilde{r}}_{14,14} = (0,0,-0.070)^T$	$\vec{\tilde{e}}_{14} = (1,0,0)^T$
15	0.0	0.0	0.0	0.0	$\vec{\tilde{r}}_{15,15} = (0,0,0.0001)^T$; $\vec{\tilde{r}}_{15,16} = (0,0,-0.0001)^T$	$\vec{\tilde{e}}_{15} = (0,1,0)^T$
16	30.85	0.15140	0.13700	0.02830	$\vec{\tilde{r}}_{16,16} = (0,0,0.34)^T$; $\vec{\tilde{r}}_{16,17} = (0,0.2,-0.06)^T$; $\vec{\tilde{r}}_{16,19} = (0,-0.2,-0.06)^T$	$\vec{\tilde{e}}_{16} = (1,0,0)^T$
17	2.07	0.00200	0.00200	0.00022	$\vec{\tilde{r}}_{17,17} = (0,0,-0.154)^T$; $\vec{\tilde{r}}_{17,18} = (0,0,0.154)^T$	$\vec{\tilde{e}}_{17} = (1,0,0)^T$
18	1.14	0.00250	0.00425	0.00014	$\vec{\tilde{r}}_{18,18} = (0,0,-0.132)^T$	$\vec{\tilde{e}}_{18} = (1,0,0)^T$
19	2.07	0.00200	0.00200	0.00022	$\vec{\tilde{r}}_{19,19} = (0,0,-0.154)^T$; $\vec{\tilde{r}}_{19,20} = (0,0,0.154)^T$	$\vec{\tilde{e}}_{19} = (-1,0,0)^T$
20	1.14	0.00250	0.00425	0.00014	$\vec{\tilde{r}}_{20,20} = (0,0,-0.132)^T$	$\vec{\tilde{e}}_{20} = (-1,0,0)^T$

$$S^M:\ P = H(q)\cdot\ddot{q} + h(q,\dot{q}) \tag{27.46}$$

$$S_a^i:\ \dot{x}_c^i = A_c^i x_c^i + b_c^i N(u^i) + f_c^i P_c^i \tag{27.47}$$

The mechanical structure of n DOFs is powered by m actuators. Since the $n - m$ joints are unpowered, the driving torques P^i about the axes of these joints are assumed to be zero, i.e., the vector of driving torques P has the following form $P = (P_c^1, P_c^1, ..., P_c^m, 0, ..., 0)^T$. In order to apply the method for stability analysis, we shall arrange the model in another way. The model of the ℓ-th unpowered joint follows from Equation (27.46):

$$-H_{\ell\ell}\ddot{q}_N^\ell = \sum_{\substack{j=1 \\ j\neq\ell}} H_{\ell j}\ddot{q}^j + h_\ell(q,\dot{q}) \tag{27.48}$$

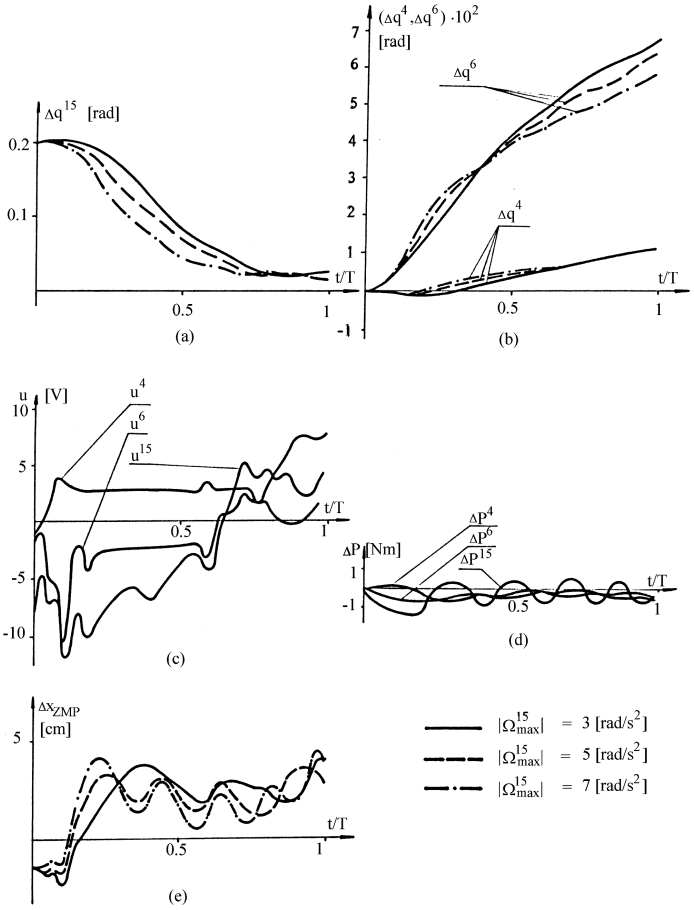

FIGURE 27.23 Walk simulation with local feedback gains defined by Equation (27.37) and with no feedback with respect to ZMP position, $\Delta q^{15}(0)=0.2[rad]$.

where $q_N^l \in R^1$ is the angle of the ℓ-th unpowered joint, $H_{\ell j}$ are the members of the matrix H(q), and h_ℓ is the member of the vector *h*. The subscript *N* denotes the unpowered DOF. However, instead of this model, let us describe the motion of the system about the axis of the ℓ-th unpowered joint as the motion of an inverted pendulum. The equation of the inverted pendulum motion in a plane is:

$$\ddot{q}_N^\ell = \frac{M}{I_o + M\rho^2} g \sin q_N^\ell + \frac{1}{I_o + M\rho^2} P_N^\ell \tag{27.49}$$

where M and I_o are the mass and inertia moment of the pendulum (the pendulum corresponds to the whole system), ρ is the distance from the supporting point to the pendulum mass center, and $P_N^\ell \in R^1$ is the resultant generalized force acting on the pendulum. If the angle q_N^ℓ is small, we can introduce the approximation $\left(\sin q_N^\ell\right) \approx q_N^\ell$. If the term multiplying q_N^ℓ is denoted by $c_o^{\ell *}$, and the term multiplying P_N^ℓ by $\bar{f}_N^\ell$, and $x_N^\ell = \left[q_N^\ell, \dot{q}_N^\ell\right]^T$ is adopted as state vector, then Equation (27.49) can be written in the matrix form:

$$\begin{bmatrix} \dot{q}_N^\ell \\ \ddot{q}_N^\ell \end{bmatrix} = \begin{bmatrix} 0 & 1 \\ c_o^{\ell *} & 0 \end{bmatrix} \begin{bmatrix} q_N^\ell \\ \dot{q}_N^\ell \end{bmatrix} + \begin{bmatrix} 0 \\ \bar{f}_N^\ell \end{bmatrix} P_N^\ell \tag{27.50}$$

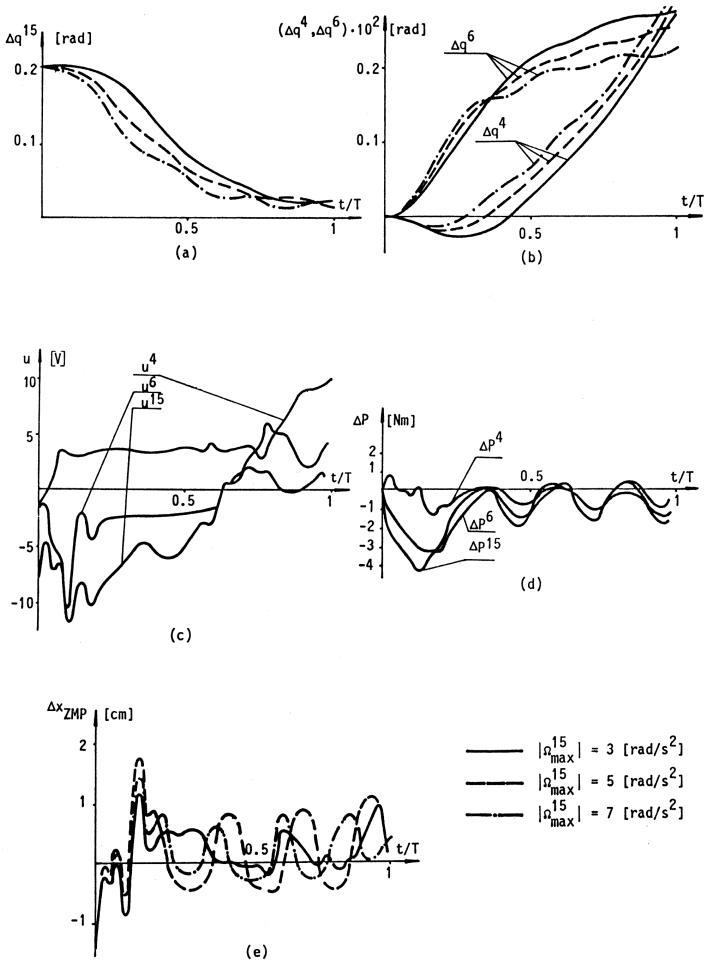

FIGURE 27.24 Walk simulation with added compensation for ZMP position (compensation is performed by ankle joint), $k_{ZMP}^{Gk}=0.5$, $\Delta q^{15}(0)=0.2[rad]$.

and in compact form

$$\dot{x}_N^\ell = A_N^\ell x_N^\ell + f_N^\ell P_N^\ell$$

Since we want the models (27.50) and (27.48) to coincide, we shall define the force P_N^ℓ as:

$$P_N^\ell = \frac{-H_{\ell\ell}^{-1}}{f_N^\ell}\left[\sum_{\substack{j=1\\ j\neq\ell}}^{n} H_{\ell j}\ddot{q}^j + h_\ell\left(q\ ,\dot{q}\ \right)\right] - \frac{C_o^{\ell *}}{\bar{f}_N^\ell} q_N^\ell \tag{27.51}$$

In this way we ensure that Equation (27.50) is an exact model of the system motion about the axis of the unpowered joint. Let us now form the composite subsystem containing one unpowered DOF (Equation (27.50)) and the *k*-th powered DOF (Equation (27.47)):

$$\begin{bmatrix}[\dot{x}_N^\ell]\\ [\dot{x}_c^k]\end{bmatrix} = \begin{bmatrix}[A_N^\ell] & 0\\ 0 & [A_c^k]\end{bmatrix}\begin{bmatrix}[x_N^\ell]\\ [x_c^k]\end{bmatrix} + \begin{bmatrix}[f_N^\ell] & 0\\ 0 & [f_c^k]\end{bmatrix}\begin{bmatrix}P_N^\ell\\ P_c^k\end{bmatrix} + \begin{bmatrix}0\\ [b_c^k]\end{bmatrix} N\left(u^k\right) \tag{27.52}$$

The subscript N corresponds to the unpowered and subscript c to the powered DOFs. Here, $x_N^\ell \in R^{n_N^\ell}$ and $x_c^k \in R^{n_c^k}$ are the state vectors of the ℓ-th unpowered $x_N^\ell = \left(q_N^\ell, \dot{q}_N^\ell\right)$ k-th powered DOFs $x_c^k = \left(q_c^k, \dot{q}_c^k, i_R^k\right)$, i_R^k is the rotor current of the corresponding DC motor, and $n_N^\ell = 2$ and $n_c^k = 3$ are their orders. $A_N^\ell \in R^{n_N^\ell x n_N^\ell}$, $A_c^k \in R^{n_c^k x n_c^k}$, $f_N^\ell \in R^{n_N^\ell}$, and $f_c^k \in R^{n_c^k}$, $P_N^\ell \in R^1$, and $P_c^k \in R^1$ are the system matrices, force distribution vectors, and generalized forces of the unpowered and powered DOFs, respectively. A_N^ℓ and f_N^ℓ are defined by Equation (27.50). Taking into account the form of the actuator matrix A_c^k and the form of the unpowered DOF (Equation (27.50)), expression (27.52) can be written as:[13,22]

$$\begin{bmatrix} \begin{bmatrix} \dot{q}_N^\ell \\ \ddot{q}_N^\ell \end{bmatrix} \\ \begin{bmatrix} \dot{q}_c^k \\ \ddot{q}_c^k \\ \dot{i}_R^k \end{bmatrix} \end{bmatrix} = \begin{bmatrix} \begin{bmatrix} 0 & 1 \\ c_o^{\ell *} & 0 \end{bmatrix} & \begin{matrix} 0 & 0 & 0 \\ 0 & 0 & 0 \end{matrix} \\ \begin{matrix} 0 & 0 \\ 0 & 0 \\ 0 & 0 \end{matrix} & \begin{bmatrix} 0 & 1 & 0 \\ 0 & a_{2,2}^k & a_{2,3}^k \\ 0 & a_{3,2}^k & a_{3,3}^k \end{bmatrix} \end{bmatrix} \begin{bmatrix} \begin{bmatrix} q_N^\ell \\ \dot{q}_N^\ell \end{bmatrix} \\ \begin{bmatrix} q_c^k \\ \dot{q}_c^k \\ i_R^k \end{bmatrix} \end{bmatrix} + \begin{bmatrix} 0 & 0 \\ \bar{f}_N^\ell & 0 \\ 0 & 0 \\ 0 & \bar{f}_c^k \\ 0 & 0 \end{bmatrix} \begin{bmatrix} P_N^\ell \\ P_c^k \end{bmatrix} + \begin{bmatrix} 0 \\ 0 \\ 0 \\ 0 \\ \bar{b}_c^k \end{bmatrix} N\left(u^k\right) \quad (27.53)$$

where $a_{i,j}^k$ are the elements of the matrix A_c^k or, in a compact form:

$$\dot{x}_z^k = A_z^k \cdot x_z^k + f_z^k \cdot P_z^k + b_z^k \cdot N(u^k) \qquad \forall k \in J$$

where $x_z^k \in R^{n_z^k}$ is the state vector of the composite subsystem, and $A_z^k \in R^{n_z^k x n_z^k}$, $f_z^k \in R^{n_z^k x 2}$, and $b_z^k \in R^{n_z^k}$ are the subsystem matrix, matrix of force distribution and vector of control distribution, respectively. Thus, $n_z^k = n_N^\ell + n_c^k$, $x_z^k = \left(x_N^{\ell T}, x_c^{kT}\right)^T$, and $P_z^k = \left(P_N^\ell, P_c^k\right)^T$. Obviously, Equation (27.53) defines only the k-th composite subsystem model. The set J is defined as J = {j, j = 2 m-n+1, …, m}. It is assumed that the k-th powered joint is associated with the ℓ-th unpowered joint.

In the stability analysis, all decoupled subsystems must be exponentially stable. If the subsystem corresponds to the joints of the kinematic chain, their coupling is represented by the moments about the joint axis. In fact, decoupling means an investigation of the subsystem model without the term that corresponds to the generalized force. In case of a composite subsystem this term is $\left(f_z^k \cdot P_z^k\right)$, i.e., the decoupled composite subsystem can be written as:

$$\dot{x}_z^k = A_z^k x_z^k + b_z^k N\left(u^k\right). \quad (27.54)$$

The interaction between these DOFs is the only way to control the motion of the unpowered DOFs. To preserve the integrity of the decoupled composite model, some additional elements should be introduced into the matrix A_z^i in the places representing the influence of powered DOFs on the unpowered DOFs and vice versa. The model of the composite subsystem has the final form:[13,22]

$$\begin{bmatrix} \begin{bmatrix} \dot{q}_N^\ell \\ \ddot{q}_N^\ell \end{bmatrix} \\ \begin{bmatrix} \dot{q}_c^k \\ \ddot{q}_c^k \\ \dot{i}_R^k \end{bmatrix} \end{bmatrix} = \begin{bmatrix} \begin{bmatrix} 0 & 1 \\ c_o^{\ell *} & 0 \end{bmatrix} & \begin{matrix} 0 & 0 & 0 \\ \left[D_1^{1k} & D_1^{2k} & D_1^{3k}\right] \end{matrix} \\ \begin{matrix} 0 & 0 \\ \left[D_2^{1k} & D_2^{2k}\right] \end{matrix} & \begin{bmatrix} 0 & 1 & 0 \\ 0 & a_{2,2}^k & a_{2,3}^k \\ 0 & a_{3,2}^k & a_{3,3}^k \end{bmatrix} \end{bmatrix} \begin{bmatrix} \begin{bmatrix} q_N^\ell \\ \dot{q}_N^\ell \end{bmatrix} \\ \begin{bmatrix} q_c^k \\ \dot{q}_c^k \\ i_R^k \end{bmatrix} \end{bmatrix} + \begin{bmatrix} 0 & 0 \\ \bar{f}_N^\ell & 0 \\ 0 & 0 \\ 0 & \bar{f}_c^k \\ 0 & 0 \end{bmatrix} \begin{bmatrix} P_N^\ell - \dfrac{D_1^k \cdot x_c^k}{\bar{f}_N^\ell} \\ P_c^k - \dfrac{D_2^k \cdot x_N^\ell}{\bar{f}_c^k} \end{bmatrix} + \begin{bmatrix} 0 \\ 0 \\ 0 \\ 0 \\ \bar{b}_c^k \end{bmatrix} N\left(u^k\right) \quad (27.55)$$

or

$$\dot{x}_z^k = A_z^{k*} x_z^k + f_z^k P_z^{k*} + b_z^k N\left(u^k\right).$$

The vector $D_1^k = \left[D_1^{1k}\, D_1^{2k}\, D_1^{3k}\right]$ represents the influence of the powered DOF on the unpowered one, whereas $D_2^k = \left[D_2^{1k}\, D_2^{2k}\right]$ represents an opposite effect. Since the vectors D_1^k and D_2^k are chosen arbitrarily, $D_1^k \cdot \left[x_k\right]^T$ and $D_2^k \cdot \left[x_n^\ell\right]^T$ will be subtracted from $\left(f_z^k\ P_z^k\right)$, i.e., $P_z^{k*} = \left(P_N^{\ell*}, P_c^{k*}\right)$, $P_N^{\ell*} = P_N^\ell - \left[\left(D_1^k \cdot x_c^k\right) / \overline{f}_N^\ell\right]$, and $P_c^{k*} = P_c^k - \left[\left(D_2^k \cdot x_N^\ell\right) / \overline{f}_c^k\right]$.

The composite subsystem model formed in this way is suitable for stability investigation and enables the stability analysis of a system having joints without actuators. It should be emphasized that the models of composite subsystems (27.55) are exact, i.e., they contain no approximations. The model (27.55) coincides with the original model of the ℓ-th unpowered joint (27.48) and the model of the *k*-th powered joint with the actuator (27.47) that is driving the *k*-th joint. We rearranged the model in order to present it in a more convenient form. The mathematical model of the mechanism part that consists of composite subsystems is

$$\dot{x}_z = \hat{A}_z^* x_z + f_z P_z^* + b_z N(u_z) \tag{27.56}$$

where $x_z \in R^{N_z}$ is the state vector; $x_z = \left(x_z^{(2m-n+1)T}, \ldots, x_z^{mT}\right)^T$. $\hat{A}_z^* \in R^{N_z \times N_z}$, $\hat{A}_z^* = diag\left\{A_z^{k*}\right\}$ is the system matrix, while $b_z = diag\left\{b_z^k\right\}$ and $f_z = diag\left\{f_z^k\right\}$, $b_z \in R^{N_z \times (n-m)}$, are the distribution matrices of control force; $N(u_z) \in R^{n-m}$ and $P_z^* \in R^{2(n-m)}$ are the corresponding control and force defined by Equation (27.55), N_z and is the order of the model formed of composite subsystems:

$$N_z = \sum_{k=2m-n+1}^{m} n_z^k . \tag{27.57}$$

Thus, the mathematical model of a complete biped mechanism S with the composite subsystems included, can be obtained by uniting the model of composite subsystems (Equation (27.56)) and the powered DOFs:

$$\text{S:}\quad \dot{x} = Ax + FP + BN(u) \tag{27.58}$$

where $x \in R^N$, $x = (x_c^{1T}, \ldots, x_c^{(n-m)T}, x_z^T)^T$ is the system state vector $P = (P_c^1, P_c^2, \ldots P_c^{2m-n}, P_z^{*2m-n+1}, \ldots, P_z^{*m})^T$. Matrices $A \in R^{N \times N}, B \in R^{N \times m}$, and $F \in R^{N \times n}$ are $A = \begin{bmatrix} \hat{A}_c & 0 \\ o & \hat{A}_z \end{bmatrix}$, $B = \begin{bmatrix} \hat{b}_c & 0 \\ 0 & b_z \end{bmatrix}$, $F = \begin{bmatrix} \hat{f}_z & 0 \\ 0 & f_z \end{bmatrix}$ $N = N_z + \sum_{i=1}^{2m-n} n_i$, $\hat{A}_c = diag\left[A_c^i\right]$, $\hat{b}_c = diag\left[b_c^i\right]$, and $\hat{f}_c = diag\left[f_c^i\right]$, $\forall i \in I_2$, $I_2 = \left\{i, i = 1, \ldots, 2m-n\right\}$.

The complete system S (Equation (27.58)) is composed of *m* subsystems: (2 *m* – *n*) subsystems correspond to the powered joints modeled as in Equation (27.47), and (*n* – *m*) composite subsystems modeled as in Equation (27.56). In fact, all the subsystems can be written in the same form:

$$\dot{x}^i = A^i x^i + b^i N(u^i) + f^i \hat{P}_i(x), \qquad \forall i \in I_1 \tag{27.59}$$

where x^i stands for x_c^i if i = 1,2, …, 2 $m - n$, and x_z^i if i = 2$m - n$ + 1, …,m. The same holds for A^i, b^i, f^i, and u^i, while $\hat{P}_i$ stands for P_c^i if i = 1,2, …, 2 $m - n$, and for P_z^{i*} if i = 2$m - n$ + 1, …, m. The order of the subsystems (Equation (27.59)) is denoted by n_i (though it might be either n_i or n_z^i, depending on i). Thus, we obtain a model of the system S in a form convenient for the application of the chosen method for stability analysis.

27.4.2 Stability Analysis

In regard to biped locomotion systems, the most suitable stability analysis seems to be the definition of practical stability.[13,22] Accordingly, the system is considered to be practically stable if $\forall x(0) \in X^I$ implies $x(t) \in X^F$, $\forall t \in T_s$ where $T_s = \{t : t \in (\tau_s, \tau)\}$ and $x(t) \in X^t(t)$, $\forall t \in T$, where $X^I \subseteq X^t(0)$ and $X^F \subseteq X^t(t)$, $\forall t \in T_s$.

Let us consider the overall system model S defined as in Equation (27.59), which can be considered as a set of m subsystems S^i (of the composite or powered joints) coupled through the term $\left(f^i \cdot \hat{P}_i\right)$.[13,22]

$$\dot{x}^i = A^i x^i + b^i N(u^i) + f^i \hat{P}_i(x) , \qquad \forall i \in I_1 .$$

Let us assume the nominal trajectory of the state vector $x^\circ(t)$, $\forall t \in T$ be given in such a way that it satisfies $x^\circ(0) \in X^I$, $x^\circ(t) \in X^F$, $\forall t \in T_s$, and $x(t) \in X^t(t)$, $\forall t \in T$. Further, let us assume the nominal trajectory $x^\circ(t)$ has been selected in such a way that we can find a nominal (programmed) control $u^\circ(t)$, which is a function of time, and which satisfies:

$$\dot{x}^{\circ i} = A^i x^{\circ i} + b^i N(u^{\circ i}) + f^i \hat{P}_i^\circ(x^\circ) , \qquad \forall i \in I_1 , \ \forall t \in T \tag{27.60}$$

where $x^\circ(t) = \left(x^{\circ 1T}(t), x^{\circ 2T}(t), \ldots, x^{\circ mT}(t)\right)^T$, $u^\circ = \left(u^{\circ 1}, u^{\circ 2}, \ldots, u^{\circ m}\right)^T$. $\hat{P}_i^\circ(x^\circ)$ denotes the nominal values of $\hat{P}_i(x)$. Because the subsystems (27.59) include the composite subsystems, the nominal trajectory $x^\circ(t)$ satisfies the composite subsystems. We assume that the nominal trajectory $x^\circ(t)$ and the corresponding nominal control $u^\circ(t)$, satisfying Equation (27.60), can be determined. However, due to the perturbation actions acting upon the system, a deviation of the system state from its nominal trajectory must appear. The model of deviation from the nominal trajectory can be written according to (27.59) and (27.60) as:

$$\Delta\dot{x}^i = A^i \Delta x^i + b^i N(t, \Delta u^i) + f^i \Delta\hat{P}_i(t, \Delta x, x^\circ(t)), \ \forall i \in I_1 \tag{27.61}$$

where $\Delta x^i = x^i - x^{\circ i}(t)$, $\Delta u^i = u^i - u^{\circ i}(t)$, $\Delta\hat{P}_i = \hat{P}_i - \hat{P}_i^\circ(x^\circ)$. The problem is to stabilize the model of deviation (27.61) from the nominal trajectory $x^\circ(t)$, i.e., we have to synthesize the control Δu^i such that the model of deviation from $x^\circ(t)$ (27.61) is stabilized. The aim is to ensure practical stability of the system around the nominal trajectory $x^\circ(t)$, so that for each $\Delta x(0) \in X^I - x^\circ(0)$, the conditions $\Delta x(t) \in X^F - x^\circ(t)$, $\forall t \in T_s$, and $\Delta x(t) \in X^t(t) - x^\circ(t)$, $\forall t \in T$ are fulfilled.

Let us synthesize a decentralized control. Consider an approximate model of deviation in its decoupled form (i.e., the model in which the coupling terms between subsystems $(f^i \Delta\hat{P}_i)$ are neglected):

$$\Delta\dot{x}^i = A^i \Delta x^i + b^i N(t, \Delta u^i) , \qquad \forall i \in I_1 . \tag{27.62}$$

The decoupled model of the system (Equation (27.62)) represents a set of decoupled linear subsystems that can be stabilized by simple linear feedback control:

$$\Delta u^i = -k_i^{LT} \Delta x^i \,, \qquad \forall i \in I_1 \tag{27.63}$$

where $k_i^L \in R^{n_i}$ is the vector of local feedback gains selected so that the subsystem:

$$\Delta \dot{x}^i = (A^i - b^i k_i^{LT}) \Delta x^i = \tilde{A}^i \Delta x^i \,, \qquad \forall i \in I_1 \tag{27.64}$$

(where $\tilde{A}^i$ is a closed-loop subsystem matrix) is exponentially stable. In (27.64), we neglected the amplitude saturation upon the input $N(t, \Delta u)^i$. If this nonlinearity is taken into account, the subsystem Equation (27.64) is exponentially stabilized in the finite region X_i in the state space with a desired stability degree Π_i. If the decoupled subsystems Equation (27.64) are considered, it is obvious that this model will be exponentially stable in the region:[13,17]

$$X = X_1 \times X_2 \times \ldots \times X_n \,. \tag{27.65}$$

We shall analyze stability of the overall system (27.61) when the decentralized control (27.63) is applied. Let us express the subsystems characteristics by the Lyapunov functions, which, with their derivatives along with solutions for decoupled subsystems, have to satisfy:[2,13,23]

$$\Pi_{i1} \left\| \Delta x^i \right\| < V_i(\Delta x^i) < \Pi_{i2} \left\| \Delta x^i \right\| \tag{27.66}$$

$$-\Pi_{i3} \left\| \Delta x^i \right\| < \dot{V}_i\left(\Delta x^i\right) < -\Pi_{i4} \left\| \Delta x^i \right\| \quad \text{along solution of (27.64)} \tag{27.67}$$

for $\forall i \in I_1$, $\Pi_{ik} > 0$ are real numbers for k = 1,2,3,4, $V_i \rangle 0$, $V_i : R^{n_i} \to R^1$. The analysis concerning the stability on finite regions using the aggregation–decomposition method can be conservative. Functions V_i should be chosen to represent the best estimates of the degree of exponential stability Π_1 of the decoupled subsystems. Thus, we should select such Lyapunov function V_i that satisfies:[13,17]

$$\dot{V}_i\left(\Delta x^i\right) = \left(grad\, V^i\right)^T \Delta x^i \le -\Pi_{i4} \Pi_{i2}^{-1} V_i \le -\Pi_i V_i \,, \qquad \forall i \in I_1 \tag{27.68}$$

where $\dot{V}_i$ is taken along the trajectory of the decoupled subsystem (27.64). Let us select the Lyapunov function in the form:

$$V_i = \left(\Delta x^{iT} H^i \Delta x^i\right)^{1/2} \,, \qquad \forall i \in I_1 \tag{27.69}$$

where the matrix $H^i \in R^{n_i \times n_i}$ (symmetric and positive definite) can be derived as the solution of the Lyapunov matrix equation:[23]

$$\tilde{A}^{iT} H^i + H^i \tilde{A}^i = -G^i \tag{27.70}$$

where $G^i \in R^{n_i \times n_i}$ is an arbitrarily defined, symmetric, and positive definite matrix. If we select G^i to be equal to $\Pi_i H^i$, then the selected Lyapunov function (27.69) obviously satisfies Equation (27.68). Since the control signal is of limited amplitude, the condition of Equation (27.68) can be satisfied only in the finite region of initial conditions $x_i(0) \in X_i$, i.e., the decoupled system is asymptotically stable in the region X defined by Equation (27.65). The region X_i can be estimated by the regions $\tilde{X}_i$ via Lyapunov functions with an appropriate choice of $V_{i\circ}$:

$$\tilde{X}_i = \left\{ \Delta x^i : V_i(\Delta x^i) < V_{i\circ} \ \ and \ \ \Delta x^i \in X_i \right\} \ , \quad \forall i \in I_1 \ , \ \ \tilde{X}_i \subseteq X_i \tag{27.71}$$

where $V_{i\circ} > 0$ are positive numbers. Then, the region:

$$\tilde{X}(0) = \tilde{X}_1 \times \tilde{X}_2 \times \ldots \times \tilde{X}_m, \qquad \tilde{X}(0) \subseteq R^N \tag{27.72}$$

is the best estimate of the region of asymptotic stability X of the set of decoupled subsystems (27.64). However, in Equation (27.64) we neglected the coupling terms $\left(f^i \cdot \Delta\hat{P}_i\right)$.

We should investigate how coupling influences the stability of the overall system S. Since $\lim_{\Delta x \to 0} \Delta\hat{P}_i \to 0$, the coupling influence can be estimated by the numbers ξ_{ij} $\left(\xi_{ij} \geq 0 \ \ for \ \ i \neq j\right)$ satisfying:[24]

$$(grad V_i^T)\, f^i \, \Delta\hat{P}_i(t\ , \Delta x) \leq \sum_{j=1}^{m} \xi_{ij} V_j \ , \qquad \forall i \in I_1 \ , \quad \forall t \in T \ , \ \forall \Delta x \in \tilde{X} - x^\circ(t) \ . \tag{27.73}$$

A sufficient condition for asymptotic stability of the overall system S in the region $\tilde{X}(0)$ is:[25]

$$GV_o < 0 \tag{27.74}$$

where V_o is the m × 1 vector and $V_o = (V_{1o}, \ldots, V_{mo})^T$, $V_o \in R^m$, and the elements of the m × m matrix G are defined as:

$$G_{ij} = -\Pi_i \delta_{ij} + \xi_{ij} \tag{27.75}$$

where δ_{ij} is the Kronecker symbol.

It is necessary to point out that Equation (27.74) is a sufficient but not necessary condition. If this condition is not fulfilled, we cannot say anything about the system stability. If Equation (27.74) is fulfilled, then $\tilde{X}(0)$ is an estimate of the region of the overall system stability. It is possible to estimate the region $\tilde{X}(t)$ that contains the system state during the tracking of the nominal trajectory $x^\circ(t)$ by:

$$\max_{i \in I}(V_i(\Delta x^i(t)) / V_{i0}) < \max_{i \in I}(V_i(\Delta x^i(0)) / V_{i0}) \exp(-\beta t) \tag{27.76}$$

where $\beta > 0$ can be computed from:

$$\beta = \min_{i \in I}(-V_{i0}^{-1} \sum_{j=1}^{m} G_{ij} V_{j0}) = \min_{i \in I}(\beta_i) \tag{27.77}$$

where $\beta_i = -V_{i0}^{-1} \sum_{j=1}^{m} G_{ij} V_{j0}$.

The inequality (27.76) is an estimation of shrinkage of the region $\tilde{X}(t)$ that contains a solution of the system S. Now the practical stability of the system can be checked out. If

$$X^I \subseteq \tilde{X}(0) \ \ and \ \ \tilde{X}(t) \subseteq X^t(t) \ , \quad \forall t \in T, \ \ \tilde{X}(t) \subseteq X^F(t) \ , \quad \forall t \in T_s \tag{27.78}$$

is satisfied, then the system S is practically stable around $x^o(t)$. If the local linear feedback controllers defined by Equation (27.63) are not sufficient to stabilize the system, an additional control input should be introduced. We may introduce the global control in the form (we use $\Delta\hat{P}_i^*$ instead of ΔP_c^{i*}):

$$\Delta u_i^G = k_{i4}^G \Delta \hat{P}_i^* + k_{i5}^G \tag{27.79}$$

where k_{i4}^G and k_{i5}^G are the scalar gains defined by Equation (27.38). $\Delta \hat{P}_i^*$ represents a quantity that corresponds to the coupling $\Delta \hat{P}_i$. By measuring forces at the contact point of the sole of the supporting leg and the ground, we get information on the effects of coupling upon the unpowered joint ΔP_N^ℓ. Therefore, we can establish a global control from the unpowered joint to the one of the powered joints (i.e., to its actuator) and compensate for the effects of coupling upon the unpowered joint. If a global control is introduced, the stability analysis can be performed as described above. However, the numbers ξ_{ij}^* estimating coupling are now defined to satisfy [instead of (27.73)] the following condition:[13,17]

$$(grad\, V_i)^T f^i \Delta \hat{P}_i + \left(grad\, V_i\right)^T b^i \Delta u_i^G \le \sum_{j=1}^{m} \xi_{ij}^* V_j\,, \quad \forall i \in I_1\,, \forall t \in T\,, \quad \forall \Delta x \in \tilde{X} - x^\circ(t)\,. \tag{27.80}$$

The next step is to check the conditions (27.74), i.e., to test whether the system with the applied local and global control is asymptotically stable in the region $\tilde{X}(0)$. The ξ_{ij} in Equation (27.75) must be replaced by ξ_{ij}^*. If the global control is properly selected, ξ_{ij}^* must satisfy:

$$\xi_{ij}^* \le \xi_{ij}, \ \forall i, j \in I_1\,.$$

Therefore, the fulfillment of stability test is easier when the global control is introduced than if only the local control is applied.

27.4.3 Example

The scheme of the locomotion mechanism is the same as in Figure 27.22. Each powered joint is modeled as one subsystem; the composite subsystem comprises the models of one powered and one unpowered joint. The inactive DOFs are not included in the subsystem modeling. To make the examples of stability analysis easier to follow, a redrawn scheme of the same mechanism is presented in Figure 27.25, with only those DOFs that will be included in the stability analysis. All the joints represented by the unit rotational axes $\vec{e}_i'$ (i = 1, . ., 9) and the corresponding links are renumbered. The link representing the upper body comprises the trunk and both hands. We shall investigate system stability in the sagittal plane only, so that there is only one unpowered DOF. Thus, the mechanism considered here has nine DOFs (n = 9), and eight of them (m = 8) are powered. The elements of matrices of the actuator models and their distribution per joint are given in Table 27.3.

The nominal trajectories are synthesized using the prescribed synergy method. The control input to the *i*-th actuator consists of two parts:

$$u^i = u^{oi} + \Delta u^i \tag{27.81}$$

where u^{oi} is the nominal control input to the *i*-th actuator while Δu^i is the corrective input to the same actuator, synthesized at the level of perturbed regimes. The control law (27.37) holds for the subsystems i = (1, 2, . ., $2m - n$), and a similar control is derived for the composite subsystems, taking into account that $\Delta \hat{P}_i^*$ values for the composite subsystems are the (2×1) vectors.

In Equation (27.37), the part depending only on local states of the *i*-th joint corresponds to the local and the rest to the global control. The global control is introduced in the form of feedback with respect to both the driving torques $\Delta \hat{P}_i^*$, and the part k_{i5}^G. $\Delta \hat{P}_i^*$ represents the force feedback (i.e., the measured moments about joints). Additional feedback with respect to the ZMP position defined by Equation (27.45) is also available.

Let us determine the stability region X_i of the decoupled subsystem. Consider first the local control (27.37 and 27.38) that has to stabilize the decoupled subsystem. If we assume that the

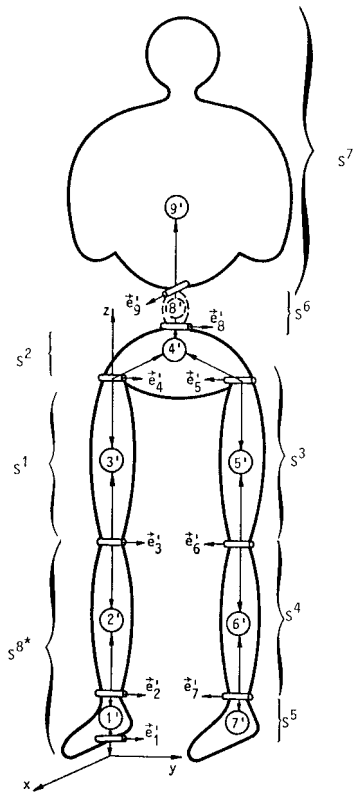

FIGURE 27.25 Simplified scheme of mechanical biped structure with disposition of the modeled subsystems.

TABLE 27.3 Actuator Parameters

	Term						
Actuator	$a_{2,2}$	$a_{2,3}$	$a_{3,2}$	$a_{3,3}$	b_3	f_2	Used at joint
M_1	–3.0	0.13	-10^5	–450	2000	$-7 \cdot 10^{-4}$	2, 3, 6, 7
M_2	–1.928	4.03	–6800	–264	400	–0.179	4, 5, 8, 9

complete state vector Δx^i is measurable, the closed-loop subsystem is given by (27.64). In the case of a stable subsystem, the poles must be at the left-hand side of the complex plane. If we denote the modulus of their real part by $|\sigma_p^i|$, the subsystem will be exponentially stable with a stability degree defined as:

$$\Pi_i = \min_{p=1,2,3} |\sigma_p^i| \tag{27.82}$$

which can be guaranteed only if the control inputs are within the limits:

$$|k_i^{LT} \Delta x^i| < \bar{u}_m^i = u_m^i - \max_{t \in T} |u^{\circ i}(t)| \ . \tag{27.83}$$

The actuator velocity–torque characteristics limit the values of the state coordinates. In view of these characteristics we can write:

$$|\bar{k}_i^2 \Delta \dot{q}^i + \bar{k}_i^3 \Delta i_R^i| \le \bar{k}_m^i \rightarrow |\bar{k}_i^T \Delta x^i| \le \bar{k}_m^i \tag{27.84}$$

where $\bar{k}_i = (0, \bar{k}_i^2, \bar{k}_i^3)^T$ and $\bar{k}_m^i$ are defined by the motor characteristics. Further, the regions of allowable angle deviations for each DOF are introduced. In this way, the stability regions are constrained for both the powered and composite subsystems.

We may define a finite region X_i (according to (27.65)) in the state space R_i^n, in which the subsystem S^i is exponentially stable with a stability degree Π_i:

$$X_i = \left\{ \Delta x^i, \left| k_i^{LT} \Delta x^i \right| < \left| \bar{u}_m^i \right| \wedge \left| \bar{k}_i^T \Delta x^i \right| \le \bar{k}_m^i \right\}. \tag{27.85}$$

To investigate the stability of the whole system, the Lyapunov subsystem functions must be chosen according to Equation (27.69), taking into account the relation (27.68), which has to be satisfied in the region X_i. $\tilde{X}_i$ will be the estimate of X_i according to:

$$\tilde{X}_i = \left\{ \Delta x^i : V_i(\Delta x^i) \le V_{i\infty} \right\}, \qquad \forall i \in I_1 .$$

To investigate asymptotic stability of the overall system, the values ξ_{ik}^*, which estimate the subsystem coupling, have to be determined according to Equation (27.80). The expression for the composite subsystem is of the form:[13,22]

$$(grad\, V_i)^T \left[f_z^i \Delta P_z^{i*}(t, \Delta x) - b_z^i (k_{i4}^G \cdot \Delta \hat{P}_i^* + k_{i5}^G) \right] \le \sum_{k=1}^{m} \xi_{ik}^* V_k \,,\ i = 2m - n + 1, \ldots, m$$

where the global control by both ΔP_N^ℓ and ΔP_c^i is introduced. If for ξ_{ij}^* thus defined, the condition (27.74) is satisfied, it can be claimed that region $\tilde{X}$, defined by (27.72), is an estimate of the region of the overall system stability.

We will form the composite subsystem model of the models of the unpowered DOFs and ankle joint. The powered subsystem model S^1 corresponds to the model of joint 3 powered by the actuator, S^2 corresponds to joint 4, S^3 to joint 5, S^4 to joint 6, S^5 to joint 7, S^6 to joint 8, S^7 to joint 9. The last model of the powered subsystem, S^8, will be included in the composite subsystem. Thus, the model of joint 2 with the model of the corresponding actuator corresponds to S^8. The model of composite subsystem will be denoted S^{8*} and will comprise the models of the unpowered subsystem and S^8. The composite subsystem matrices A_z^{8*} and f_z^8 and vector b_z^8 are defined as:

$$A_z^{8*} = \begin{bmatrix} 0 & 1 & 0 & 0 & 0 \\ 0.882 & 0 & -80 & -10 & 0 \\ 0 & 0 & 0 & 1 & 0 \\ 300 & 100 & 0 & -3 & 0.13 \\ 0 & 0 & 0 & -100000 & -450 \end{bmatrix}, \quad f_z^8 = \begin{bmatrix} 0 & 0 \\ 0.01387 & 0 \\ 0 & 0 \\ 0 & 0.0007 \\ 0 & 0 \end{bmatrix}, \quad b_z^8 = \begin{bmatrix} 0 \\ 0 \\ 0 \\ 0 \\ 2000 \end{bmatrix}.$$

The vectors from Equation (27.55) are $D_1^8 = [-80, -10, 0]$ and $D_2^8 = [300, 100]$. The Lyapunov functions of all subsystems are selected in the form of Equation (27.69). The matrices H^i are selected to satisfy Equation (27.70) and they are obtained as:

$$H^8 = \begin{bmatrix} 100422\ .00 & 33545\ .10 & 8660\ .65 & -98\ .68 & 0.02 \\ 33545.10 & 11425.23 & -3273.52 & -335.46 & -0.07 \\ 8660.65 & -3273.52 & 183099.94 & 8965.84 & 1.95 \\ -98.68 & -335.46 & 8965.84 & 1097.767 & 0.086 \\ 0.02 & -0.07 & 1.95 & 0.086 & 0.0009 \end{bmatrix}.$$

The Lyapunov matrices corresponding to the models of powered subsystems S^i are:

$$H^i = \begin{bmatrix} 62777.42 & 2291.71 & 0.56 \\ 2291.71 & 161.15 & 0.02 \\ 0.56 & 0.02 & 0.00011 \end{bmatrix} \quad i = 1, 4, 5 \quad H^i = \begin{bmatrix} 32912.207 & 408.621 & 4.535 \\ 408.621 & 6.482 & 0.065 \\ 4.535 & 0.065 & 0.00092 \end{bmatrix} \quad i = 2, 3, 6, 7.$$

The regions of joint angle deviations (the superscripts correspond to the subsystems model numbers) in which stability is investigated are (in radians):

$$\Delta q^1 = \pm 0.044, \quad \Delta q^2 = \pm 0.0422, \quad \Delta q^3 = \pm 0.0126, \quad \Delta q^4 = \pm 0.03,$$

$$\Delta q^5 = \pm 0.03, \quad \Delta q^6 = \pm 0.099, \quad \Delta q^7 = \pm 0.01, \quad \Delta q_z^1 = \pm 0.01, \quad \Delta q_z^2 = \pm 0.077$$

where Δq_z^1 and Δq_z^2 correspond to the joints comprising the composite subsystem, i.e., the unpowered and powered DOFs (the ankle joint with the axis of rotation $\vec{e}_2$).

The constants V_{io} defining the estimates of the stability regions $\tilde{X}_i$ are computed as:

$$V_{30} = 0.65, \quad V_{20} = 1.0399, \quad V_{30} = 0.4256, \quad V_{40} = 0.1545,$$

$$V_{50} = 0.75166, \quad V_{60} = 0.7395, \quad V_{70} = 0.1814, \quad V_{80} = 0.3291 .$$

The constant V_{8o} corresponds to the composite subsystem. The results of stability analysis are presented in Table 27.4. Three types of control laws are investigated:

1. The complete feedback structure defined by Equation (27.37) plus the global control with respect to ZMP displacement defined by Equation (27.44).
2. The local control is introduced (the corresponding gains k_{i1}^L, k_{i2}^L, and k_{i3}^L are defined in (27.38) plus global control with respect to ZMP position (27.44).
3. Only local control from Equation (27.37) is introduced.

Table 27.4 presents results (matrix G, and vectors Gv_o and η) for all three control laws. The first three rows correspond to laws 1 through 3, respectively. The first and second groups of three rows each correspond to the hip and knee of the supporting leg. The third, fourth, and fifth groups represent the hip, knee, and ankle of the leg in swing phase. The sixth and seventh groups correspond to trunk motion in the frontal and sagittal planes. The last group of three rows represents the composite subsystem.

To draw a final conclusion about system stability, the product $G_o \cdot V_o$ must be observed. If this product is negative, the stability under the given conditions is proved. The vector η represents shrinkage of the bounds of the regions $\tilde{X}(t)$.

27.5 Realization of Anthropomorphic Mechanisms and Humanoid Robots

Locomotion activity, especially the human gait, belongs to a class of highly automated motion. Bernstein[26] was the first to comprehend this fact. Humans have at their disposal to achieve complete skeletal (locomotion–manipulation) activity several hundred muscles that allow over 300 equivalent DOFs. In view of the high number of biological actuators through which humans exercise motor activity, the imitation of this activity seems to be a hopelessly difficult task. Understanding the mechanisms of gait control and other skeletal activities is extremely difficult, especially if one bears in mind the necessarily detailed insight into the multilevel structures to

TABLE 27.4 Results of Stability Analysis (Composite System Consisting of Ankle and Unpowered Joint)

$$G = \begin{bmatrix}
-53.92 & 0 & 0 & 0 & 0 & 0 & 0 & 0 \\
-50.91 & 0 & 0 & 0 & 0 & 0 & 0 & 0 \\
-50.91 & 0 & 0 & 0 & 0 & 0 & 0 & 0 \\
0 & -2404.16 & 0 & 0 & 0 & 0 & 0 & 0 \\
0 & -2360.11 & 0 & 0 & 0 & 0.172 & 0.003 & 0 \\
0 & -2360.11 & 0 & 0 & 0 & 0 & 0 & 0 \\
6.021 & 0 & -76.15 & 0 & 0 & 0 & 0 & 0 \\
6.491 & 0 & -73.88 & 0 & 0 & 0 & 0 & 0 \\
6.491 & 0 & -73.88 & 0 & 0 & 0 & 0 & 0 \\
0 & 0 & 0 & -5114.02 & 0 & 0 & 0 & 0 \\
0 & 0 & 0 & -4761.15 & 0 & 0 & 0 & 0 \\
0 & 0 & 0 & -4761.15 & 0 & 0 & 0 & 0 \\
0 & 0 & 0 & 0 & -789.58 & 0 & 0 & 0 \\
0 & 0 & 0 & 0 & -764.16 & 0 & 0 & 0 \\
0 & 0 & 0 & 0 & -764.16 & 0 & 0 & 0 \\
6.351 & 0 & 0 & 0 & 0 & -67.56 & 0 & 0 \\
6.767 & 0 & 0 & 0 & 0 & -66.40 & 0 & 0 \\
6.767 & 0 & 0 & 0 & 0 & -66.40 & 0 & 0 \\
0 & 0.89 & 0 & 0 & 0 & 0 & -32.84 & 0 \\
0.045 & 1.547 & 0 & 0 & 0 & 0.198 & -28.86 & 0.109 \\
0.045 & 1.547 & 0 & 0 & 0 & 0 & -28.86 & 0.109 \\
1.236 & 16.534 & 0 & 16.375 & 7.77 & 11.14 & 70.52 & -218.31 \\
1.544 & 17.505 & 0 & 20.465 & 6.93 & 11.99 & 67.1 & -216.53 \\
3.242 & 22.87 & 3.8 & 43.052 & 2.29 & 16.72 & 47.86 & -206.7
\end{bmatrix}$$

$$G \cdot v_O = \begin{bmatrix}
-110.81 & -1564.4 & -20.03 & -790.28 & -593.5 & -36.91 & -5.38 & -34.82 \\
-104.63 & -1535.6 & -18.1 & -735.75 & -574.4 & -35.2 & -3.95 & -32.93 \\
-104.63 & -1535.6 & -18.1 & -735.75 & -574.4 & -35.2 & -3.95 & -20.84
\end{bmatrix}^T$$

$$\eta = \begin{bmatrix}
53.92 & 2404.16 & 47.08 & 5114.01 & 789.6 & 49.9 & 29.64 & 98.04 \\
50.91 & 2359.92 & 42.54 & 4761.14 & 764.16 & 47.6 & 21.78 & 92.7 \\
50.91 & 2359.92 & 42.54 & 4761.14 & 764.16 & 47.6 & 21.78 & 58.67
\end{bmatrix}^T$$

control human locomotion and manipulation activity. Despite these challenges, technological advances have allowed us to create mechanical counterparts to humans that are capable of performing some human tasks. This section will briefly describe active anthropomorphic mechanisms and humanoid robots.

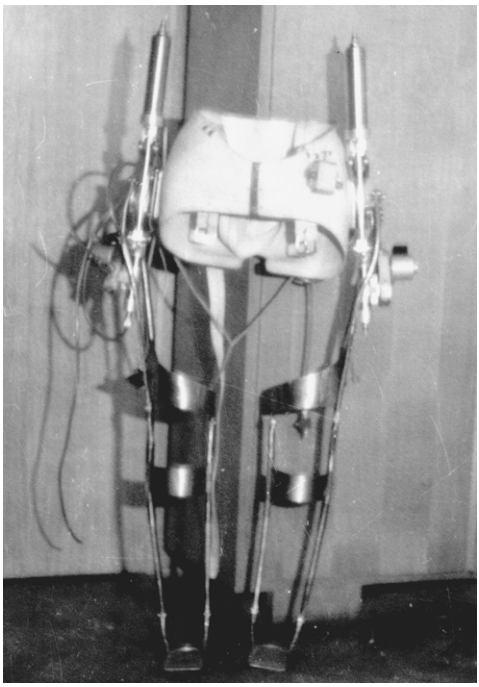

FIGURE 27.26 Kinematic walker (1969).

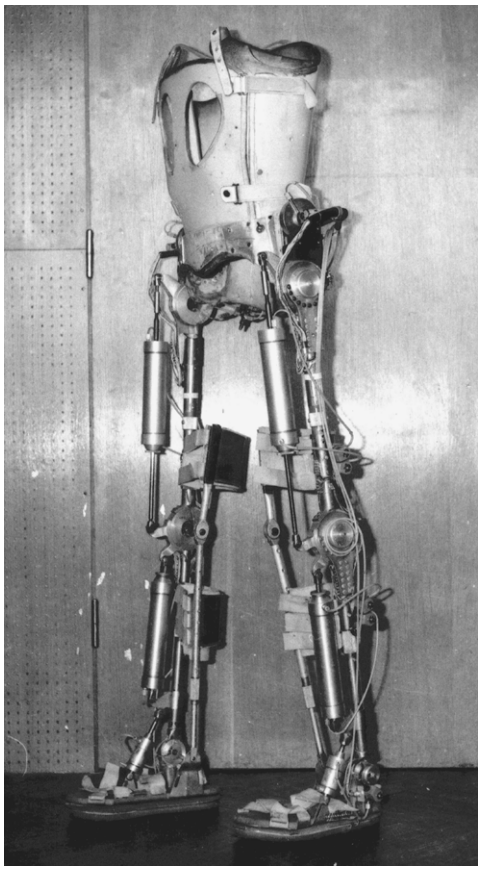

FIGURE 27.27 Complete pneumatically driven active exoskeleton.

27.5.1 Active Exoskeletons

The first pneumatically driven active anthropomorphic exoskeleton (Figure 27.26) was created in 1969 at the Mihajlo Pupin Institute (Belgrade).[13] Each leg had its own drive consisting of only one pneumatic cylinder, which, through kinematic linkage, actuated also the knee, while the foot was passive. The device produced a sliding-foot gait.

After this first attempt of anthropomorphic gait the researchers in the Robotics Laboratory of the Mihajlo Pupin Institute also developed new models of partial and complete exoskeletons dedicated to the restoration of basic locomotion activities of paraplegics. A complete pneumatically driven active exoskeleton for rehabilitation use was developed and manufactured in 1972.[13,27,28] It is depicted in Figure 27.27.

The first experiments with these exoskeletons were successfully carried out at the Belgrade Orthopedic Clinic during 1972 and 1973. It was concluded in 1973 that further development of pneumatically driven active exoskeletons for rehabilitation was not promising because of poor energy autonomy provided by the pneumatic source of energy. The decision was made to switch to the development of an active exoskeleton with electromechanical drives.[13,27,28]

In 1974, the first electromechanical active exoskeleton (Figure 27.28) was realized. It included a number of sophisticated solutions in the design of the exoskeleton structure. In addition to the basic motion of the leg in the sagittal plane, the hip joint performed two kinematically programmed

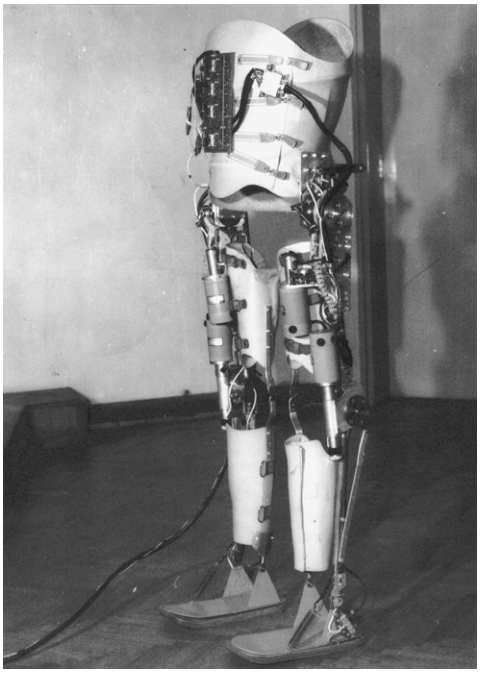

FIGURE 27.28 Complete electromechanical exoskeleton.

motions, pelvic twist and sideways motion, to achieve more stable and quasi-realistic gait. When this exoskeleton type was realized, light batteries were not available to power the devices and computer technology was in its pre-microprocessor stage. For these reasons, the power source and control system were outside the exoskeleton, and this greatly limited the utility of the device.

However, it should be pointed out that the above technological limitations have been overcome. An early conception of artificial gait for rehabilitation purposes, having in mind the real possibility of active exoskeleton autonomy with respect to control and energy, will be realizable in a much more successful way.

27.5.2 Humanoid Robots

High expectations accompanied the appearance of robots for personal use. Such robots coexist with humans and provide support for the aged and the physically handicapped.

An anthropomorphic form of robot is usually expected when the robot is intended for personal use. A human-like or humanoid robot that works with humans as a partner in the living environment needs to share the same workspace and possess the common thinking and behavioral modes of humans. A humanoid robot will integrate information from its sensors and coordinate its actions to realize high level and natural communication with humans by using speech, facial expression, and body motion.

The Waseda University has been one of the leading research centers working on anthropomorphic robots since I. Kato and his colleagues started the WABOT (WAseda roBOT) project and produced the first biped walking robot, WABOT-1, in 1973 (Figure 27.29).[29]

In 1984, A. Takanishi and his co-workers developed a hydraulic biped robot (Waseda Leg 10 Refined Dynamic or WL-10RD) that was able to walk dynamically. By 1985, their dynamic biped had the ability to walk on slopes and stairs. Takanishi's group achieved compensation by lower limbs and trunk in 1986. They introduced an effective computation algorithm to obtain the periodic

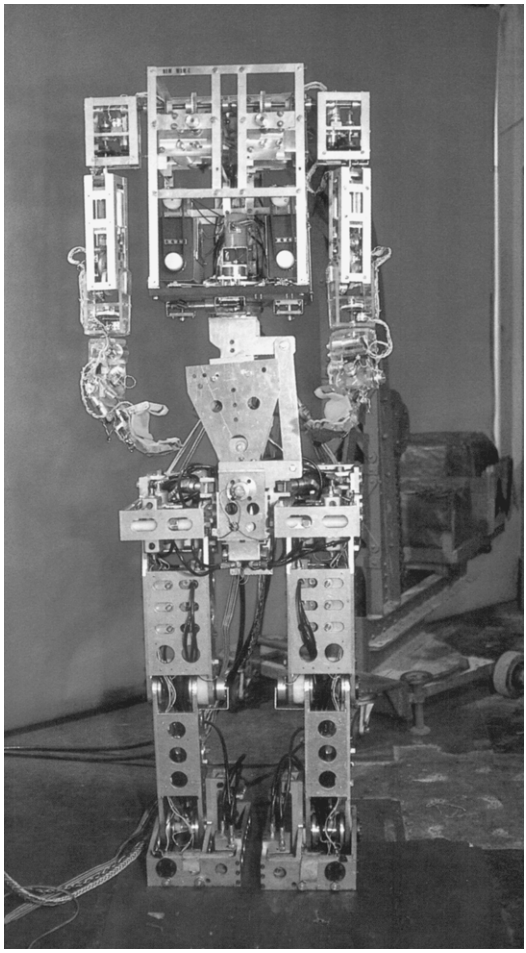

FIGURE 27.29 WABOT-1 (1973).

upper-body trajectory from the arbitrarily preset ZMP and leg trajectories. Their work was the first example of implementation of the ZMP concept into a humanoid robot. The WL-12 series robots achieved dynamic walking and turning under conditions of unknown external forces and on unknown surfaces (Figure 27.30).

Takanishi and his co-workers also developed a bipedal humanoid robot called WABIAN (WAseda BIpedal humANoid) and the method of its control (Figure 27.31). They accomplished the following design goals: (1) develop an electrically powered bipedal humanoid robot having upper limbs, a three DOF trunk, and a head (the total number of active DOFs is 35), (2) devise a motion pattern-generating program to study overall cooperative motion, and (3) support the effectiveness of a dynamic walking system that allows walking, dancing with the motion of the three DOF trunk and upper limbs, carrying of a load with both hands, and continuous bipedal walking in human living space based on a closed-loop dynamic walking control method.[29,31]

The most successful representation of a humanoid robot is the Honda humanoid robot.[32] The goal was to develop a robot capable of coexisting and collaborating with humans and performing tasks that humans cannot perform. Honda wanted to develop a new robot to meet consumers' needs — not a robot limited to specialized operations. Such a robot is capable of moving around the house, encountering various obstacles such as staircases, doors, furniture, etc.

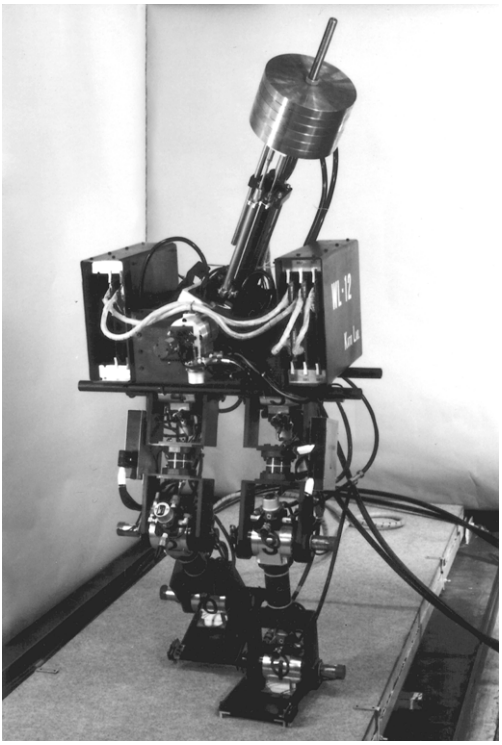

FIGURE 27.30 Dynamic walking with a compensating body: WL-12 (1986).

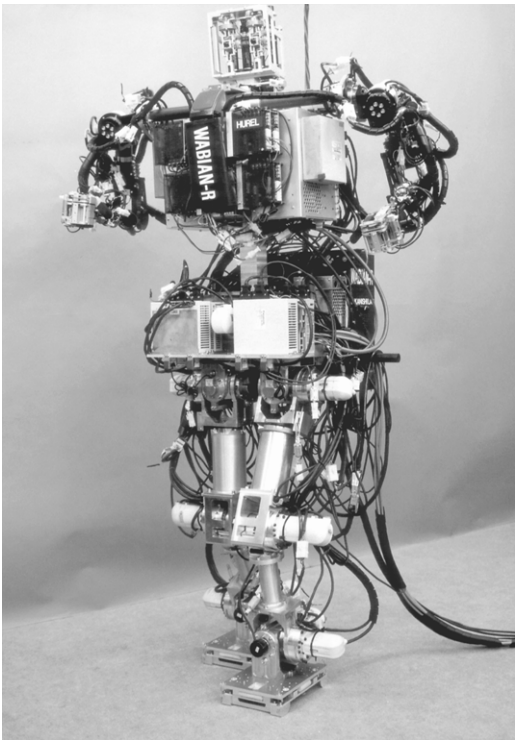

FIGURE 27.31 Bipedal humanoid robot WABIAN.

The legs of the Honda robot have 12 DOFs and the redundant arms have 14 DOFs. The hand is similar to a two-finger gripper with two DOFs. The head has two DOFs, bringing the total number of DOFs to 32 (Figure 27.32). Honda developed several types of biped robots. The maximum walking speed achieved by a specialized robot was 4.7 km/h. To maintain dynamical equilibrium and stabilize the perturbed work regime of the robot, Honda concluded that the robotic system required a body inclination sensor and a ground reaction sensor for each foot. The inclination sensor consists of three accelerometers and three angular speed sensors (optical fiber gyros). It is also used as a navigation sensor. Each foot and wrist has a six-axis (three component forces and three component moments) sensor. The robot is also equipped with an impact absorption mechanism to damp the landing impact ground reaction force. The overall height of the robot is 1820 mm, its width is 600 mm, and it weighs 210 kg.

To recover the robots's posture, the ground reaction force control shifts the total ground reaction force to an appropriate position by adjusting each foot's desired position and posture. Model ZMP is used to control the shifting of the desired ZMP to an appropriate position in order to recover posture. The foot landing position control corrects the relative position of the upper body and feet in conjunction with the ZMP control. By having the three controls working simultaneously Honda has realized the robot with a posture stabilizing control similar to that of the human.

Honda has continued its research on biped walking humanoid robots. In 2000, it developed the ASIMO (Advanced Step in Innovative Mobility) humanoid robot.[33] It has an overall height of 1200 mm, weighs 43 kg, and has 26 DOFs. The robot is compatible with human living environments. The walking technology includes behavior prediction such that the robot can change its walking motion freely and smoothly without interruption. A central role in the control strategy is played by the model ZMP control.

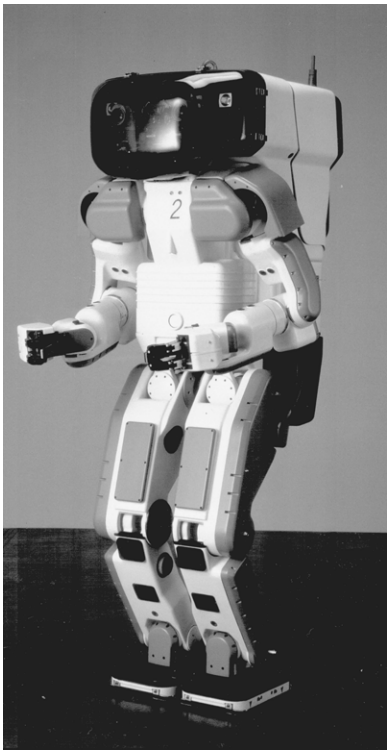

FIGURE 27.32 Honda humanoid robot P2.

27.5.3 Virtual Humanoid Robot Platform

Nakamura and Takanishi and a group of associates developed the most complete software tool for modeling and control of humanoid robots reported to date. They developed a simulator of humanoid robots and a controller of whole body motion.[34] The basic modules of this software include:

1. A *dynamic simulator* that executes efficient dynamics and kinematics and can accomodate structure changes of any open or closed kinematic chain, and even such kinematic chains as to change connectivity in operation. The connectivity change function is essential because it is often seen when a humanoid walks, touches or holds the environment, grasps an object with the both hands, and is even connected with another humanoid.
2. A *view simulator* or image synthesis that consists of modeling, illumination, shapes and materials of objects in a scene, and cameras. The shapes of artificial objects can be obtained from CAD data, but it is hard to produce material models of surfaces. The simulator can generate sequences of the fields of view from the eyes of the robot according to the dynamics simulation. When the view simulator is integrated with the dynamics simulator, visual feedback of humanoid robots can be simulated.
3. A *humanoid motion controller* that can handle biped locomotion, dynamic balance control at the standing position, and collision avoidance.

As part of the Virtual Humanoid Robot Platform (V-HRP) project, a motion controller has been developed to achieve biped locomotion adaptive to terrain, including walking straight, turning, going up or down the stairs, and walking on rugged ground.[34] With this programming library, complex locomotion can be realized as a sequence of basic motion patterns. The link between the basic motions of the robot is automatically generated for continuous motion control. Control data

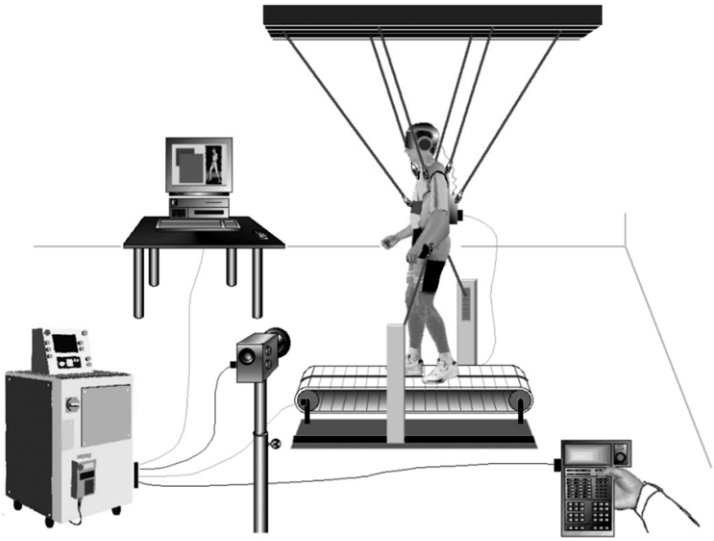

FIGURE 27.33 Global RehaRob concept.

for a walk adaptable to terrain generated by the library have been examined and found to be consistent with the mechanism's dynamics obtained using a dynamics simulator. The data's consistency has also been proven by experiment using the hardware model developed to verify the compatibility of the simulation model with the real world.

Concerning this module, two examples were presented. In the first example the robot is standing on two legs, and both legs are controlled in the same manner. With the proposed balance control, the robot can successfully sit down, reach the ground with its arms, and stand up again. To demonstrate 3-D balance, a kicking motion was tested. The robot can fully swing its left leg in one second while balancing with its right leg. With the proposed control, the robot is capable of successful kicking and balancing. The motions of the arms and body were added to provide a natural appearance. All compensation is done by the ankle actuators of the supporting leg.

These software modules are integrated via CORBA (Common Object Request Broker Architecture). This enables Internet clients to use the software. The modules are implemented as CORBA servers, and a client can utilize them if the servers are accessible via the IIOP (Internet Inter Orb Protocol).

The developers of the Humanoid Robot Platform expect it to be "the common base of humanoid robotics research focusing on software development for the community."

27.5.4 New Application of the ZMP Concept in Human Gait Restoration

A novel application of ZMP for human gait rehabilitation using treadmill training and partial body weight bearing (PWB) has been proposed.[12] This methodology has recently been successfully used for gait recovery by stroke patients.[35]

One of the Wisa-ROMED projects endowed by the Fraunhofer Community developed a demonstration system referred to as RehaRob which represents the first application of the ZMP concept for evaluation and control of the human gait. The RehaRob is a powerful robotic system for supporting gait rehabilitation and restoration of motor functions. It combines the advantages of PWB with a number of robotic and humanoid control functions. Safe, reliable, and dynamically controlled weight suspension and posture control systems support patients and allow them to autonomously recover their gaits early in the rehabilitation stage.

The global RehaRob architecture is presented in Figure 27.33. The system consists of an active weight-relieving robotic system (wire robot) that performs partial dynamic weight compensation

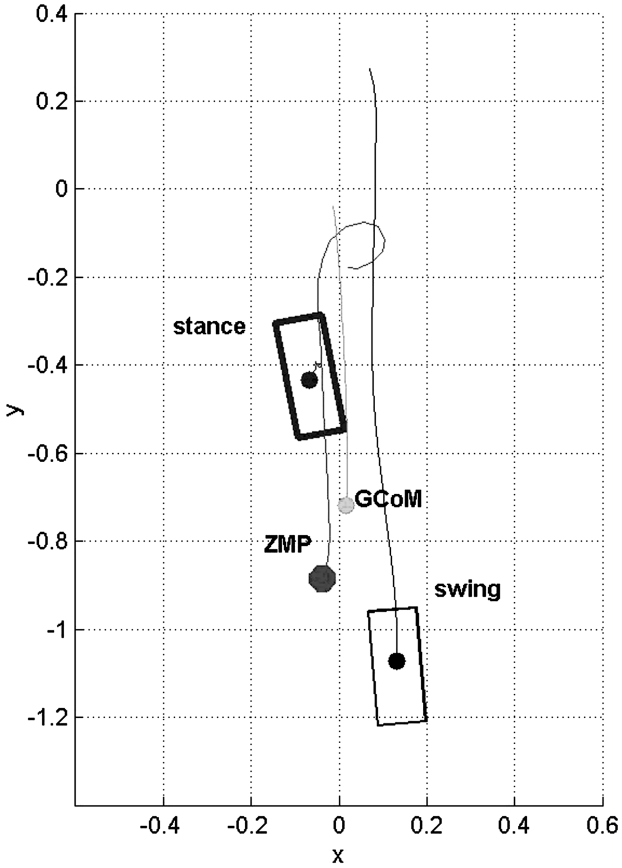

FIGURE 27.34 ZMP and GCoM trajectories during single limb phase.

and posture control synchronously with the human lower limb motion; a harness system (patient interface); a treadmill and/or lifting system axial motion device (for rehabilitation of orthopedic patients) that supports repetitive motion progression; a sensory system (motion camera, insole pressure sensors, force sensors, inclinometers, wire position sensors) that collects data about the human gait and provides feedback to the control system; a system controlling the wire robot, treadmill (the axial motion system), rehabilitation planning, and programming system (user interface); an AR or VR system providing visual feedback; computer safety control; and a mechanical system providing exception-handling functions.

The robot wires are connected to the trunk and pelvis at optimized attachment points (in the system under development, a total of ten wires are applied). The robot exerts active external forces upon the trunk and pelvis to reduce the weight on the lower limbs (reaction force) and balance the posture, thus essentially supporting the gait. Redundant wires are needed to ensure tension in all wires independent of dynamic loads. The rigid trunk–pelvis system connected by a spherical joint has nine DOFs.

The RehaRob control is based on the ZMP concept. It utilizes wire force, foot reactions measurements, and a model of wire robot and human interaction to estimate and control ZMP. The application of the human motion ZMP trajectory for controlling a biped robot has recently been proposed.[36] For body modeling, the RehaRob uses a rigid model of a human developed with MATLAB (MatMan). The model has 37 DOFs. Figure 27.34 presents the results of simulation of the ZMP and ground projection of CoM (GCoM) trajectories for the human gait during stance phase (stance and swing legs are denoted in the figure). Apparently, in a period of time the ZMP is within the stance foot supporting area, while in the remaining time it leaves this area following

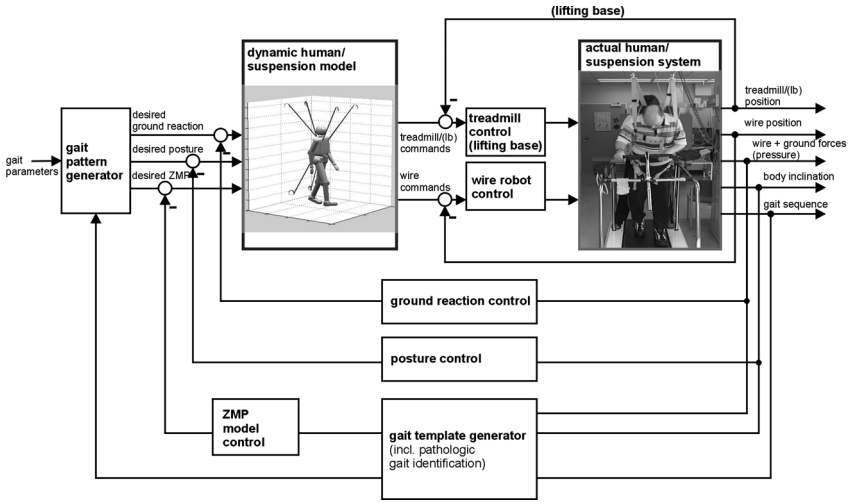

FIGURE 27.35 RehaRobot control concept.

the moving swing foot. In a stable gait, the ZMP remains within the enveloping area constrained by foot projections on the ground.

Unlike the ZMP model of human/humanoid walking (Equation 27.7), the RehaRob system includes additional wire-active forces affecting the equilibrium conditions (27.2). By means of the wire forces, it is possible to control both body reaction and ZMP location.

The motion of the relevant upper and lower limbs (e.g., knee) affecting system dynamics can be measured by relatively inexpensive sensors. The trunk and pelvis positions in the RehaRob system are directly measured and controlled using both wires and body sensors. To cope with model inaccuracies and ZMP estimation errors, the RehaRob system implements a relatively complex control structure closing several control loops (Figure 27.35) around reaction force and gait posture and uses the internal wire robot and treadmill control. This control scheme includes the basic gait pattern generator (initial contact, stance, swing, single limb), which, based on the captured gait state and required weight suspension percentage generates the desired ground reaction, as well as nominal posture and ZMP location data. These values are compared with the measured (i.e., estimated) ones, and the control feedback is closed around the dynamic human gait and wire robot models. This provides the inputs to the internal wire and treadmill control loops (treadmill velocity, pulley position, and wire forces). The local controllers control the wire robot system so that the posture can support and follow the joint motion of the desired walking pattern. This pattern is a combination of ideal walking patterns (templates) including desired weight suspension and the subject's gait performance estimated using the sensory system. Gait balance is achieved by the ZMP and posture controls for the generated pattern. The gait template generator includes data about the subject's abnormal gait, as well as the emergency and exception-handling strategies (to compensate for 100% weight upon the stance leg if the conditions for single-leg support are not available, for example, due to improper ankle or knee joint position, etc.). This control scheme is similar to the recent humanoid control approaches proposed in Hirai et al.[32] and Yamaguchi et al.[37]

27.6 Conclusion

Having at our disposal limited space in a thematically widely conceived handbook, it was a difficult task to present such a broad and attractive field of scientific and professional interest (one recently experiencing tremendous impetus) in a way that would be both an introduction and offer in-depth coverage of humanoid robotics.

Because of this, some new challenging aspects and dilemmas concerning humanoid robotics had to be omitted, as well as new views on its current importance and role in the future. Some examples include issues such as the new frontiers of humanoid robotics, human–humanoid interactions, using humanoid robots to study human behavior, humanoid features in public places, a neurobiological perspective on humanoid robot design, humanoid robot cognition. Because the character of *Mechanical Design Handbook: Modeling, Measurement, and Control* is mostly determined by dynamics, dynamic control, and advanced design diverse types of objects and systems, the authors believe they need to mention, at least briefly, some of the phenomena pertaining to humanoid robots that deserve detailed studies to make these robots more suitable for use.

The above mostly relates to refining the trajectory of the zero-moment point, especially when the gait passes from the single-support to the double-support phase. It is then that the introduction of the semi-rigid foot, in contrast to its rigid version, offers the possibility of a more faithful representation of the perturbation state of the humanoid robot to prevent the robot instantaneously reaching its foot edge — the case that has been considered up to now.

Further very important improvements are related to a more reliable description of the constraint environment model, which enables more realistic insight into robot–environment interactions that offer the possibility of control dynamic performance, e.g., by reducing the dynamic impact of the robot's foot at the end of the swing phase, which is achieved by applying active dampers at the ankle joint contstruction, as well as by passive or semi-active dampers at the other joints of the mechanical construction.

Finally, let us emphasize once more that the gait of humanoid robots is an extremely complex contact task involving a mobile object whose dynamics include interaction with its environment's dynamics, which means that (among other things) it is necessary to ensure simultaneous control with respect to both position and contact force. Some preliminary results indicate justification of such an approach, [38,39] whereas more extensive results will be achieved by a more faithful analysis of dynamic contact and the synthesis of the appropriate laws of simultaneous dynamic position force control.[40]

References

1. Vukobratović, M. and Juričič, D., Contribution to the synthesis of biped gait, *IEEE Trans. Biomedical Eng.,* 16(1), 1969.
2. Juričič, D. and Vukobratović, M., *Mathematical Modeling of Biped Walking Systems,* ASME Publication 72-WA/BHF-13, 1972.
3. Vukobratović, M. and Stepanenko, Yu., On the stability of anthropomorphic systems, *Mathematical Biosciences,* 15, 1, 1972,
4. Vukobratović, M. and Stepanenko, Yu., Mathematical models of general anthropomorphic systems, *Mathematical Biosciences,* 17, 191, 1973.
5. Vukobratović, M., How to control the artificial anthropomorphic systems, *IEEE Trans. Syst., Man, Cybernetics, SMC-3,* 497, 1973.
6. Arakawa, T. and Fukuda, T., Natural motion of biped locomotion robot using hierarchical trajectory generation method consisting of GA, EP, layers, *Proc. IEEE Conf. Automation Robotics,* Albuquerque, NM, 211, 1997.
7. Inoue, K., Yoshida, H., Arai, T., and Mae, Y., Mobile manipulation of humanoids — real time control based on manipulability and stability, *Proc. IEEE Int. Conf. Robotics Automation,* San Francisco, 2217, 2000.
8. Huang, Q., Kajita, S., Koyachi, N., Kaneko, K., Yokoi, K., Arai, H., Komoriya, K., and Tanie, K., A high stability, smooth walking pattern for a biped robot, *Proc. IEEE Int. Conf. Automation Robotics,* Detroit, 65, 1999.
9. Yagi, M. and Lumelsky, Biped robot locomotion in scenes with unknown obstacles, *Proc. IEEE Int. Conf. Automation Robotics,* Detroit, 375, 1999.

10. Fujimoto, Y., Obata, S., and Kawamura, A., Robust biped walking with active interaction control between foot and ground, *Proc. IEEE Int. Conf. Robotics Automation,* Leuven, Belgium, 2030, 1988.
11. Fukuda, T., Komata, Y., and Arakawa, T., Stabilization control of biped locomotion robot base learning with GAs having self-adaptive mutation and recurrent neutral networks, *Proc. IEEE Int. Conf. Robotics Automation,* Albuquerque, NM, 217, 1997.
12. Šurdilović, D. and Bernhardt, R., Robust control of dynamic interaction between robot and human: application in medical robotics, *Proc. German Robotic Conf.,* 429, 2000.
13. Vukobratović, M., Borovać, B., Surla, D., and Stokić, D., *Scientific Fundamentals of Robotics, Vol. 7, Biped Locomotion — Dynamics, Stability, Control, and Application*, Springer-Verlag, Berlin, 1990.
14. Stepanenko, Yu. and Vukobratović, M., Dynamics of articulated open chain active mechanisms, *Mathematical Biosciences,* 28(1/2), 1976.
15. Vukobratović, M. and Stokić, D., One engineering concept of dynamic control of manipulators, *Trans. ASME J. Dynamic Syst., Meas. Control,* 102, June 1981.
16. Vukobratović, M. and Stokić, D., Is dynamic control needed in robotic systems and if so, to what extent? *Int. J. Robotics Research,* 2(2), 18–34, 1983.
17. Vukobratović, M. and Stokić, D., *Scientific Fundamentals of Robotics, Vol. 2, Control of Manipulation Robots: Theory and Application*, Springer-Verlag, Berlin, 1982.
18. Vukobratović, M. and Stokić, D., Suboptimal synthesis of robot decentralized control for large-scale mechanical systems, *IFAC Automatica,* 20(6), 803, 1984.
19. Borovać, B., Vukobratović, M., and Surla, D., An approach to biped control synthesis, *Robotica,* 7, 231–241, 1989.
20. Vukobratović, M. and Stokić, D., Significance of the force-feedback in realizing movements of extremities, Trans. Biomedical Eng., 27(12), 705, 1980.
21. Stokić, D. and Vukobratović, M., Practical stabilization of robotic systems by decentralized control, *IFAC Automatica,* 20(3), 1984.
22. Borovać, B., Vukobratović, M., and Stokić, D., Stability analysis for mechanisms with unpowered degrees of freedom, *Robotica,* 7, 349, 1989.
23. Šiljak, D.D., *Large Scale Dynamic Systems: Stability and Structure*, North-Holland, Amsterdam, 1978.
24. Morari, M., Stephanopulos, G., and Aris, R, Finite stability regions for large scale systems with stable and unstable systems, *Int. J. Control,* 26(5), 1977.
25. Weissenberger, S., Stability regions of large-scale systems, *Automatica,* 9, 653, 1973.
26. Bernstein, N.A., *On the Motion Synthesis*, Medgiz Moscow, 1947 (in Russian).
27. Vukobratović, M., Hristić, D., and Stojiljović, Z., Development of active anthropomorphic exoskeletons, *Med. Biol. Eng.*, 12(1), 1974.
28. Vukobratović, M. and Hristić, D., Active orthoses of lower extremities, *Orthopedic Technic,* 4, 1985.
29. Takanishi, A., Humanoid robots — a new tide towards the next century for natural human-robot collaboration, *Proc. Int. Conf. Humanoids,* Tokyo, 2000.
30. Takanishi, A., Ishida, M., Yamazaki, Y., and Kato, I., The realization of dynamic walking by the biped walking robot WL-10RD, *Proc. 1985 ICAR,* 459, 1985.
31. Lim, H., Ishiji, A., and Takanishi, A., Emotion based walking of bipedal humanoid robot, *Proc. 13-th CISM-IFToMM Symp. Theory Practice Robots Manipulators.* Springer-Verlag, Berlin, 295, 2000.
32. Hirai, K., Hirose, M., Haikawa, Y., and Takenaka, T., The development of honda humanoid robot, *Proc. 1998 IEEE Int. Conf. Robotics Automation,* Leuven, Belgium, 1321, May 1998.
33. Technical Review, Honda R&D, 13(1), April 2000.
34. Nakamura, Y., Hirukawa, H., Yamane, K., Kajita, S., Yokoi, K., Tanie, K., Fujie, M., Takanishi, A., Fujiwara, K., Suehiro, T., Kita, N., Kita, Y., Hirai, S., Nagashima, F., Murase, Y., Inoba, M., and Inoue, H., V-HRP: virtual humanoid robot platform, *Proc. Int. Conf. Humanoids,* Tokyo, Japan, 2000.

35. Kawamura, J., Ide, T., Hayashi, S., Ono, H., and Honda, T., Automatic suspension device for gait training, *Prosthetics and Orthotics Int.,* 120, 1993.
36. Dasgupta, A. and Nakamura, Y., Making feasible walking motion of humanoid robots from human motion capture data, *Proc. IEEE Int. Conf. Robotics Automation,* Detroit, 1044, 1999.
37. Yamaguchi, J., Soga, E., Inoue, S., and Takanishi, A., Development of a bipedal humanoid robot — control method of whole body cooperative dynamic biped walking, *Proc. IEEE Int. Conf. Robotics Automation,* Detroit, 368, 1999.
38. Park, J. H. and Chung, H., Hybrid control for biped robots using impedance control and computed torque control, *Proc. IEEE Int. Conf. Robotics Automation*, Detroit, Michigan, 1365–1370, 1999.
39. Silva, F. M. and Machado, J. A. T., Goal-oriented biped walking based on force interaction control, *Proc. IEEE Int. Conf. Robotics Automation*, Seoul, Korea, 4122–4129, 2001.
40. Vukobratović, M. and Ekalo, Yu., New approach to control of robotic manipulators interacting with dynamic environments, *Robotica*, 14, 3139, 1996.